https://dx.doi.org/10.1016/j.jcsr.2019.02.006

Behavior and design of cold-formed and hot-finished steel elliptical tubular stub columns

Yancheng Cai [a], Wai-Meng Quach [b,*], Man-Tai Chen [a], Ben Young [c]

[a] Department of Civil Engineering, The University of Hong Kong, Pokfulam Road, Hong Kong, China

[b] Department of Civil and Environmental Engineering, The University of Macau, Macau, China

[c] Department of Civil and Environmental Engineering, The Hong Kong Polytechnic University, Hong Kong, China (Formerly, Department of Civil Engineering, The University of Hong Kong, Pokfulam Road, Hong Kong, China)

Abstract

Significant progress has been made on structural behavior of hot-finished (HF) steel members with elliptical hollow sections (EHS) in the past few years. However, there is very limited research on cold-formed (CF) steel members with EHS. In this study, both CF and HF steel elliptical tubular stub columns are investigated. The investigation includes laboratory testing, numerical analysis and design evaluations. The geometric imperfection measurements, full load-end shortening relationships and load-strain curves of the stub columns are detailed in this paper. A non-linear finite element model was developed and validated against test results obtained from the present study as well as from the literature. The validated numerical model was employed to perform an extensive parametric study, where the CF and HF stub columns with EHS were carefully designed to include a broad range of the cross-section slenderness and aspect ratio. The cold-forming effect on the CF sections was taken into account in a conservative manner. The ultimate strengths obtained from the tests and numerical analysis were compared with the predictions in the design strengths predicted by the design methods proposed in the existing literature and the Direct Strength Method (DSM). The comparisons showed that the strengths predicted by the equivalent diameter method, the DSM and the modified DSM are generally conservative and reliable. The modified DSM provides the most accurate and the least scattered predictions among these design methods. Therefore, the modified DSM is recommended for the design of CF and HF steel elliptical tubular stub columns.

Keywords: Cold-formed; Direct Strength Method; elliptical hollow section; hot-finished; stub column.

* Corresponding author. Tel.: 853-8822-4358.

E-mail address: wmquach@um.edu.mo (W.M. Quach).

1. Introduction

Elliptical hollow section (EHS) is a new member to the family of hollow steel sections available to the construction industry. Its distinct closed nature brings the merits of different flexural rigidities about the two principal axes by offering efficient bending resistance about the major axis and moreover, high torsional stiffness. It can offer greater bending capacity compared with circular hollow section (CHS) of the same area, due to the existence of strong and weak axes directions as mentioned earlier, while maintaining a smooth closed shape. In addition, there is reduced visual intrusion compared to CHS, if the member is viewed from one common direction [1]. These merits of EHS have drawn considerable attention from structural engineers and architects in the construction industry. However, the design of EHS is not covered in the current international steel design specifications [2-7].

Significant progress has been made on the structural behavior of EHS steel members in the past few years. A wide range of research topics have been covered, including cross-section tests by compression [8], cross-section tests by bending and combined bending and shear [9-10], member buckling tests by compression about the minor axis and major axis [11-12], welded connection tests [13-14] and gusset plate connection tests [15-16]. It should be noted that these investigations were focused on hot-rolled and hot-finished (HF) elliptical tubular sections.

Cold-forming is another commonly used steel manufacturing technology with merits such as its high-speed manufacturing process, high-quality surface finish and close repetitive tolerance. In addition, more intricate contours and innovative cross-section shapes can be produced by cold-forming. The cold-formed (CF) EHS recently becomes available in the market but the investigation on CF steel with EHS is very limited. Recently, Quach and Young [17] has conducted an experimental investigation on both CF and HF steel EHS which possess a same virgin material and same nominal dimensions, Their results [17] shows that CF steel EHS behaves quite differently from HF steel EHS in terms of resulting material properties after forming. Chen and Young [18] has modified the Direct Strength Method (DSM) [2] for the design of CF steel stub columns with EHS based on a series of tests and numerical analyses. It should be noted that the current steel design specifications [2-7] have not yet covered the design of CF and HF steel stub columns with EHS, and the DSM has not been calibrated to the design of HF steel EHS. Up to date, there is no research focusing on the

comparison between CF and HF steel elliptical tubular stub columns in terms of structural behavior.

In this paper, investigations on the behavior of CF and HF steel elliptical tubular stub columns were carried out by laboratory testing, numerical analysis and design evaluations. The CF and HF steel EHS in the test program had an aspect ratio of 2 with a nominal section dimension ($2a \times 2b \times t$) of 200×100×6.5 mm. The geometric imperfection measurements, full load-end shortening curves and load-strain curves of the stub columns are presented in detail. A non-linear finite element model was developed and validated against test results obtained from this study as well as other literature. The validated numerical model was employed to perform an extensive parametric study, where the CF and HF steel stub columns with EHS were carefully designed to include a broad range of the cross-section slenderness and aspect ratio. The ultimate strengths obtained from the tests and numerical analysis were compared with the design strengths predicted by the design methods proposed in the existing literature and the DSM [2] since there is no codified design rule for CF and HF steel compression members with EHS. Reliability of these design predictions were studied by reliability analysis. Design recommendations are made for the CF and HF steel elliptical tubular stub columns under compression.

2. Experimental investigation

2.1. General

Two different forming processes, namely, cold-formed and hot-finished, were used to fabricate the elliptical hollow sections in the test program. The CF EHS were fabricated by rolling the structural steel sheet through a set of rollers into a circular hollow shape. The edges of the structural steel sheet were milled and the section was then closed by welding. Furthermore, the circular hollow shape was rolled into elliptical hollow shape. The entire cold-forming process was conducted at ambient temperature, except at the location of weld. The hot-finishing process is similar to the cold-forming process, except that the EHS were further heated to approximately 750 °C or higher temperature at the finishing stage in order to reduce or remove residual stresses from the produced tube. In this study, the CF steel elliptical tubular stub column (CF-SC) was fabricated by cold-forming process, while the HF steel elliptical tubular stub column (HF-SC) was fabricated by hot-finishing process.

2.2. Test specimens

The CF-SC and HF-SC specimens had the same nominal cross-section dimension in the test program. These CF and HF sections were produced from a same virgin sheet material. The nominal widths in the major axis ($2a$) and minor axis ($2b$) were 200 mm and 100 mm, respectively. Hence, these elliptical hollow sections had an aspect ratio of 2.0. The nominal plate thickness (t) of these sections was 6.5 mm. The specimens were cut from the same batch of tubes as those reported by Quach and Young [17]. The nominal length (L) of these EHS stub columns was taken as 330 mm to make sure that the specimens would not fail by overall buckling. The configuration of the EHS stub column is shown in Figure 1(a), and the relationship between a and b satisfies the equation of $(x/a)^2 + (y/b)^2 = 1$, where x and y are the coordinates along the x-x axis and y-y axis, respectively, as shown in Figure 1(b). The measured dimensions of the CF-SC and HF-SC specimens are summarized in Table 1, where the R_{max} ($R_{max} = a^2/b$) and R_{min} ($R_{min} = b^2/a$) represent the maximum radius of curvature at the flattest location and the minimum radius of curvature at the curviest location (i.e., corner) of a EHS, respectively; A means the full cross-section area; w_o and P_t indicate the measured maximum local imperfection and the tested ultimate strength of the stub column, respectively.

2.3. Tensile coupon tests

The material properties of CF and HF steel elliptical tubular sections have been investigated by tensile coupon tests in Quach and Young [17]. The coupon specimens were machined across a half of the cross-section as indicated in Figure 2. Table 2 illustrates the material properties at the flattest location (LT6), curviest (corner) location (LT1) and the mean values of material properties for half of the cross section, including initial Young's modulus (E), static 0.2% proof stress ($f_{0.2}$), static tensile ultimate strength (f_u), elongation at ultimate strength (ε_u) and elongation at fracture (ε_f) based on the 25 mm gauge length. A distinct yield strength (f_y) was found for coupon specimens extracted from the HF elliptical tubular section, and the values are also included in Table 2. Quach and Young [17] observed that materials near the curviest location and quarter location (i.e., a location at the mid way between the curviest and flattest locations) of the CF specimen possessed a greater strength enhancement than the material near the flattest location, while the mechanical properties of the HF specimen were quite uniform throughout the cross-section and similar to that of the virgin steel material. The detailed results of the coupon tests are described in Quach and Young [17].

2.4. Geometric imperfection measurements

Initial local geometric imperfection of CF and HF steel elliptical tubular stub columns were measured before conducting stub column tests. One Mitutoyo transducer with an accuracy of 0.001 mm was used to inspect the concavity/convexity at five locations along the specimens (Lines 1, 2, 3, 4 and 5) on the tube surface. Figure 3 shows the setup of the local geometric imperfection measurements. Measurements were performed longitudinally at a 5 mm interval from one end to another end of the specimen. To eliminate the possible local imperfection induced by cold-sawing [19], the measurements were started and finished 10 mm away from the ends of the specimen. The measurement procedure is identical at the five locations (1, 2, 3, 4 or 5) for all specimens. The measurements were corrected with reference to the datum taken as a straight line connecting the start and end measurement points. The concavity and convexity of the specimen profile are indicated by the positive and negative values, respectively. Figure 4 illustrates the measured local geometric imperfection profiles of the CF-SC and HF-SC specimens. The maximum measured initial local geometric imperfections of the CF-SC and HF-SC specimens are shown in Table 1.

2.5. Test setup and procedure

The test setup mainly comprised four 50 mm range Linear Variable Displacement Transducers (LVDTs) to measure the end shortening of the stub columns. A total of nineteen strain gauges were attached on each specimen to determine the axial strain and detect the initiation of local bucking, if any; among which sixteen strain gauges were located at the mid-height of the stub column with thirteen (No. 1~13) evenly distributed along a half of the cross-section and another three (No. 14~16) located at the flattest and quarters portions of another half of the cross-section as shown in Figures 5 and 6. The remaining three strain gauges (No. 17~19) were parallel to those of No. 14~16 along the length direction, but at the quarter height of the stub column. The arrangement of the strain gauges was carefully designed to reflect the differences of material properties across the sections, in particular for the CF EHS. Figure 5(a)-(b) illustrates the CF-SC and HF-SC specimens with attached strain gauges. Figure 6 shows the corresponding numbering of the strain gauges. Before testing, both ends of stub column specimens were milled flat to allow for uniform loading over the cross-section.

A typical test setup of CF-SC specimen is shown in Figure 7 (left). A servo-controlled hydraulic testing machine with a loading capacity of 5000 kN was used to apply axial compressive force to the specimens. To prevent "elephant foot" failure, a pair of steel frames together with curved steel blocks of 25 mm height was used near each end of the specimens, as shown in Figure 7 (right). Similar pair of clamping devices was used in the tests for elliptical hollow section stub columns [18] and for semi-oval hollow section compression members [19] in order to avoid premature end failure. An initial load of approximately 4.0 kN was applied to the specimens such that any possible gaps between the specimen and bearing plates were eliminated through adjusting the special bearing at the top. The bearing was then locked after proper adjustment, to ensure that the load was applied uniformly over the cross-section of the CF-SC and HF-SC specimens. The tests were conducted by driving the actuator in displacement control with a constant loading rate of 0.5 mm/min. The use of displacement control allowed the tests to be continued in the post-peak range. The applied displacement was paused for 100 s near the yielding and the ultimate load, as well as the post-ultimate load to obtain the static responses of stub column specimens. The readings of the LVDTs and strain gauges were recorded by a data logger at 1 second intervals during testing. The axial end shortening of the specimens was then obtained by the mean values of recorded data.

2.6. Test results

The tested and static load-end shortening responses of the CF-SC and HF-SC specimens are plotted in Figure 8. The ultimate strengths based on the test curves (P_t*) and the obtained static curves (P_t) as well as the corresponding end shortenings (δ_u) of the specimens at the ultimate strengths are presented in Table 3. No elastic local buckling was observed during the stub column tests. To further distinguish whether the stub column failed by cross-section yielding, the static ultimate strengths (P_t) of the CF-SC and HF-SC specimens were compared with the squash loads calculated as $Af_{0.2}$ and Af_y, respectively. The material properties at flattest portion (LT6) and the curviest portion (LT1) of cross-section area were used. It is shown that the ratios of $P_t/Af_{0.2}$ (P_t/Af_y) are greater than unity, regardless of the material properties used, as shown in Table 3. Therefore, the CF-SC and HF-SC specimens were failed by cross-section yielding. The values of $Af_{0.2}$ and Af_y by using the material properties at the flattest portion (LT6) were plotted in the static curves of Figure 8 for comparison. Figures 9(a)-(b) shows the failure mode of the CF-SC and HF-SC specimens at post-ultimate load,

respectively.

Figures 10 and 12 show the load-strain curves for the stub columns with strain readings obtained from strain gauges from No. 1 to No.13 and from No. 14 to No.19, respectively. The locations of the strain gauges are illustrated in Fig. 6. In order to look into the differences of the structural behavior, the corresponding initial parts of the whole load-strain curves were plotted, as shown in Figures 11 and 13. As shown in Figure 11(a) for Specimen CF-SC, the load-strain curves corresponding to strain gauges No. 1 and No. 13, which were located at the curviest portion of the section, show higher load levels (higher stress levels) than those of most other strain gauges under the same strain. The load-strain curve corresponding to strain gauge No. 1 shows the highest load level among the curves; while the curve corresponding to strain gauge No. 7, which was located at the flattest portion, shows the lowest load level among the curves. The load-strain curves for strain gauges No. 4 and No.7, which were located at the quarter of the section perimeter from the curviest portion, lie in between the curves for strain gauges No. 1 and No. 7. Similar findings were observed from another half section surface of Specimen CF-SC (see Figure 13(a)). As shown in Figure 13(a), the curve for strain gauge No. 15, which was located at the flattest portion, shows the lowest load level among the curves, and the curve for strain gauge No. 17 is much higher than those of other stain gauges. This is in consistence with the findings reported in Quach and Young [17] that the higher material strength $f_{0.2}$ were found near the quarter locations [17], which may be due to the local bending applied at the corresponding locations and the involvement of greater cold-forming effect. The behavior of Specimen HF-SC is different from that of Specimen CF-SC, since the cold-forming effect on Specimen HF-SC was significantly reduced by hot treatment. The yield strengths f_y of material at different locations of the HF section are close to each other across the section. As shown in Figure 11(b), the load-strain curves for strain gauge No. 7 at the flattest portion, strain gauge No. 10 at the quarter location and strain gauge No. 13 at the curviest portion are similar, although the No. 1 at another curviest portion shows a higher load level. The behavior for another half section surface is shown in Figure 13(b), where the curves obtained from the strain gauges are similar, except for those obtained from strain gauge No. 16 and No. 19, which show a slightly higher load level under the same strain. Two load-strain curves were used to determine the material properties of the CF-SC and HF-SC specimens, respectively. One is from strain gauge No. 3 for Specimen CF-SF (see Figure 6), as this load-strain curve was located nearly the average position among the 13 stress-strain curves for this specimen, as shown in Figure 11(a). Another one is from strain

gauge No. 13, which is located at the curviest portion, for Specimen HF-SC. It is because, as mentioned previously and as shown in Figure 11(b), the load-strain curves at the flattest portion, the quarter location and the curviest portion of Specimen HF-SC are similar. Therefore, these two load-strain curves were selected as the representative material properties of the EHS stub columns. The obtained material properties based on these two curves are presented in Table 4.

3. Numerical investigation

3.1. General

The finite element model (FEM) using the program ABAQUS of version 6.14 was developed to simulate the tests of CF-SC and HF-SC specimens. The FEM was firstly evaluated by sensitivity analysis, and then validated against the EHS stub column test results obtained from this study as well as the test results reported by Chan and Gardner [8].

3.2. Finite element model

The measured cross-section geometries as reported in Table 1 and the measured material properties as detailed in Quach and Young [17] were used. As mentioned earlier, the CF-SC and HF-SC specimens were cut from the same batch of steel elliptical tubes as those investigated in Quach and Young [17]. The measured engineering stress-strain curves obtained from the coupon tests were converted to the true plastic stress-strain curves, where the whole true plastic stress-strain curve was mimicked by means of a piecewise linear stress–strain model, in particular, over the strain-hardening region. Hence, the material non-linearity was incorporated into the FEM. In the FEM, the four-node shell element with reduced integration (S4R) in the ABAQUS element library was selected, which has six degrees of freedom. The S4R element has been commonly used in modeling the structural behavior of metallic tubular members [20], including CF and HF steel elliptical tubular stub columns under compression [8, 18]. The meshed steel elliptical tubular stub column using S4R element is shown in Figure 14(a).

A reference node located at the centroid of each cross-section end was defined, as shown in Figure 14 (a). The reference node was coupled with the corresponding cross-section end in

displacements and rotations. Hence, the boundary conditions of the stub columns were associated with the reference nodes at each end. The reference nodes were restrained against all degrees of freedom, except for the longitudinal displacement (along the stub column length direction) at the loading point. The elastic local buckling mode patterns were obtained by performing eigenvalue analysis in BUCKLE procedure. The buckling mode pattern was amplified by a certain magnitude of imperfection to consider the initial local geometric imperfection profile of the steel elliptical tubular stub columns. Similar to the tests conducted by displacement control, a specified axial displacement was assigned to the reference point at the loading end using a General Static analysis step. The nonlinear geometric parameter (NLGEOM) was enabled to deal with large displacement analysis.

3.3. Sensitivity analyses

The FEM was evaluated by a series of analyses to investigate the sensitivity of the parameters on the ultimate strengths of the stub columns, including the elastic eigenmode patterns, element sizes, magnitude of imperfection and material properties across the section, where tensile and compressive material properties and residual stress were considered. It should be noted that the magnitude of imperfection between CF and HF steel elliptical tubular stub columns is quite different, as shown in Figure 4. The magnitude of local imperfection was taken as $t/50$ by Chen and Young [18] and $t/100$ by Chan and Gardner [8] for the numerical study of CF and HF steel elliptical tubular stub columns, respectively. Furthermore, research conducted by Quach and Young [17] shows that there is significant differences between the material properties of CF and HF steel EHS. In the numerical study of CF EHS conducted by Chen and Young [18], in order to take into account the variation of mechanical properties across the whole cross-section, these properties were modelled in two types of regions: (1) a region of a higher strength enhancement from the curviest location (i.e., the tip of the section) to 1/6 of the cross-section depth ($2a$) was assigned with the mechanical properties of the curviest portion (associated with R_{min}); and (2) the rest of the cross-section with a smaller amount of strength enhancement was assigned with the properties of the flattest portion (associated with R_{max}). In the numerical study of HF EHS conducted by Chan and Gardner [8], the material properties at the flattest portion (associated with R_{max}) were used for the whole cross-section of EHS.

In this study, the first ten elastic eigenmode patterns were firstly studied. By taking the lower

bound of eigenvalues, the first elastic local buckling mode shape, typically in a symmetrical shape, was selected as the initial local geometric imperfection profile of the stub column. This is in consistence with the selection for the numerical studies of CF [18] and HF [8] steel EHS stub columns. The buckling mode shape was then amplified by a certain magnitude of imperfection in the analysis. Based on the numerical studies of CF [18] and HF [8] steel EHS stub columns, the effects of mesh size were studied, where mesh sizes of 5×5 mm, 10×10 mm, 13×13 mm and 20×20 mm were adopted in the model. It was found that the variation of mesh size generally has little effect on the ultimate strength of the stub column, but the post-buckling behavior. Hence, the mesh size of 10×10 mm, which is smaller than the upper bound of 20×20 mm [8], was used for the further analysis, in order to obtain the accurate results and remain the computation efficiency.

Another thirty-five analyses were then performed for the sensitivity analysis on the imperfection magnitude and material properties assignment, as shown in Table 5. Three magnitudes of imperfection were generally considered, namely, the measured maximum value w_o as reported in Table 1, the values of $t/10$ and $t/100$ that associated with the section thickness. For each imperfection magnitude, six different approaches of material properties inputs (Case 1 to Case 6) were considered, where Cases 1 and 2 for material properties of only LT1 and LT6, respectively, Case 3 for both LT1 and LT6, Case 4 for LT1 to LT11, Case 5 for material properties from stub column tests and Case 6 considering residual stresses, as detailed in the following:

- Case 1 and Case 2 represent the approaches that the material properties of the flattest portion (LT6 as shown in Figure 2) and those of the curviest portion (LT1 as shown in Figure 2) were assigned to the whole cross-section, respectively.
- Case 3 represents that the material properties of the flattest location (i.e., coupon LT6) and the curviest location (i.e., coupon LT1) were assigned to a half of the section perimeter near the flattest portion and another half near the curviest portion, respectively (see Figure 14(b).
- Case 4 represents that the material properties across the half section (from LT1 to LT11 as shown in Figure 2) were used in the portioned section shown in Figure 14.
- Case 5 represents that the material properties obtained from stub column tests were used for the whole cross-section, where the material properties are shown in Table 4.
- Case 6 is an additional case for CF steel EHS by incorporating the measured membrane residual stresses [17], which was induced by the cold-forming and welding process.

The FEM of Case 6 was based on the model of Case 4, as the residual stress corresponding to the material properties in each portion could be incorporated. It should be noted that only membrane residual stresses in the longitudinal direction were considered, as the longitudinal bending residual stresses have been inherently incorporated in the material properties obtained from the coupon tests. One additional magnitude of imperfection of $t/50$ was also considered in Case 1 since this value was found to be suitable for the numerical analysis of CF steel elliptical tubular stub columns [18].

Table 5 summarizes the results of the sensitivity analyses by comparing with the static test strengths (P_t). It is shown that an imperfection magnitude of $t/10$ led to an underestimation of P_t by 5%~8%, while the magnitude of $t/100$ led to an overestimation of P_t by 3% to 10% for the HF-SC specimen over these Cases 1-5. For the CF-SC specimen, the imperfection magnitude of $t/10$ could lead to either an underestimation of P_t up to 8% for Case 1 or an overestimation of P_t up to 5% for Case 2. The magnitude of $t/100$ specified for the CF-SC specimen resulted in good predictions of P_t in Case 1, but caused an overestimation of P_t up to 10% for Case 2. In Cases 3-6, the use of $t/100$ could lead to an overestimation of P_t up to 6% for the CF-SC specimen, while the use of $t/10$ resulted in good predictions for the same specimen. As shown by a comparison between Cases 4 and 6 (see Table 5), the inputs of longitudinal membrane residual stresses has a little effect on the ultimate strength obtained from the numerical study. Hence, the inclusion of membrane residual stresses in the FEM could be exempted for simplicity. It is also found that the inputs of measured maximum imperfection w_o did not provide a good prediction of P_t for both the CF-SC and HF-SC specimens in the same case condition (e.g., an overestimation of P_t by 2% for HF, but an underestimation of P_t by 15% for CF in Case 1). However, it is shown that the imperfection inputs of $t/50$, which was used in Chen and Young [18] for CF steel stub columns with EHS, provided the best predictions of P_t for both CF-SC and HF-SC specimens in the present study. Figure 15(a)-(b) illustrates the load-end shortening curves of the different cases with imperfection inputs of $t/100$ for specimens CF-SC and HF-SC, respectively.

3.4. Model validation and parametric study

Based on the aforementioned modeling parameters and assumptions in the sensitive analyses, the FEM using material properties at the flattest portion (LT6 as shown in Figure 2) together with the imperfection magnitude of $t/50$ was developed for both CF and HF tubes. The

developed FEM was also validated against another series of test results for CF and HF steel elliptical tubular stub columns reported in Chan and Gardner [8] and in Chen and Young [18], respectively. Table 6 shows the comparison between the ultimate strengths (P_t) from tests and the ultimate strengths (P_{FEA}) from finite element analysis (FEA), where the labels of stub specimens used in Chan and Gardner [8] and in Chen and Young [18] were directly adopted herein for simplicity. It is found that the developed FEM can successfully replicate the axial load-carrying capacities of the steel elliptical tubular stub columns as evident by the mean value and COV of (P_t/P_{FEA}) being 1.04 and 0.064, respectively. In addition, the failure mode can also be captured by the FEM as shown in Figure 9(c). Therefore, the magnitude imperfection of $t/50$, the first elastic local buckling mode shape and the material properties located at the flattest portion of the section are suggested for the finite element analysis of both CF and HF steel elliptical tubular stub columns.

The validated FEM for steel EHS stub column was further used to perform an extensive parametric study on the structural behavior of CF and HF steel elliptical tubular stub columns. The cross-section dimensions and slenderness of EHS were carefully designed to cover a wide range of fabrication factors, with a total specimen number of 102, as shown in Table 7. The larger dimension of the section ($2a$) varied from 120 to 570 mm, with the cross-section aspect ratio (a/b) of the EHS varied from 1.0 up to 3.0. In each EHS, the relationship between a and b satisfies the equation of $(x/a)^2 + (y/b)^2 = 1$. Since the expression of cross-section slenderness is not well defined in the current international design specifications [2-7], the equivalent diameter ($D_e = 2a^2/b$) proposed by Chan and Gardner [8] applicable for $1 \leq a/b \leq 4$ was adopted to examine the coverage of cross-section slenderness. The section slenderness limits ($D_e/t\varepsilon^2$) specified in EC3-1.1 [6] for circular hollow sections were used, where $\varepsilon = (235/f_y)^{0.5}$. In the calculation, the circular diameter was replaced by the equivalent diameter, and the static $f_{0.2}$ and f_y obtained from the coupon tests of LT6 at the flattest location as shown in Table 2 were used for CF and HF sections, respectively.

The dimensions of CF and HF steel elliptical tubular stub columns used in the parametric study are detailed in Tables 8-12, where the labeling reveals the section dimension of $2a \times 2b \times t$, e.g., 120×120×5. Tables 8-11 presents the section dimensions for both CH and HF steel EHS with Class 1-4 sections, respectively. It should be noted that these section dimensions were carefully selected in order to consider the cold-forming effect of CF steel EHS in a conservative manner. As mentioned earlier, the mechanical properties at the flattest portion of

the tested Specimen CF-SC had been used in the validated FEM. This validated FEM was adopted for the parametric study. The R_{max}/t for the tested Specimen CF-SC is 32.0 (see Table 1), which is an indicator of both the curvature and cold work at the flattest portion of the CF specimen. A smaller value of R_{max}/t indicates the involvement of a larger amount of cold work in a section and results in a higher strength enhancement (i.e., a higher yield strength $f_{0.2}$). Therefore, the dimensions of all the CF specimens in this parametric study were designed such that their values of $R_{max}/t \leq 32.0$ (see Tables 8-11). In this study, the use of the validated FEM (which is based on the mechanical properties at the flattest portion with $R_{max}/t = 32.0$) in the parametric study would result in conservative predictions of CF steel stub columns.

The cold-work effect on the mechanical properties of HF sections is negligible as concluded by Quach and Young [17]. Thus, the R_{max}/t is no longer related to any forming effect and material strength of HF sections. Therefore, the dimensions of HF specimens were designed to cover a wider range of section slenderness in compared with the CF specimens, regardless of the R_{max}/t value. They cover all section sizes of those CF specimens ($R_{max}/t \leq 32.0$) together with some additional cross-sectional dimensions with larger values (i.e., $R_{max}/t > 32$) The dimensions of those HF specimens with $R_{max}/t > 32$ are summarized in Table 12. The length of each stub column (both CF and HF sections) was taken to be 2.0 times the larger outer dimension of EHS, as adopted by in Chan and Gardner [8]. The results obtained from the parametric study using the verified FEM are presented in Tables 13-17.

4. Comparison of test and numerical results with predicted strengths

4.1 General

As mentioned earlier, there is no codified design rule for CF and HF steel elliptical tubular stub columns under compression. The stub column strengths obtained from tests (P_t) and FEA (P_{FEA}) were compared with the nominal strengths (unfactored design strengths) predicted by the equivalent diameter method [8]. The equivalent diameter method was previously proposed for the design of HF steel EHS, where slenderness limit in the EC3-1.1 [6] for circular hollow section were used with equivalent diameter incorporated. In addition, the DSM [2] and the recently modified DSM proposed by Chen and Young [18] were also examined. Unlike the equivalent diameter method, the section classification is not necessary for the DSM [2]. The DSM [2] uses full cross-section area instead of effective area in the design calculation. It

should be noted that the DSM [2] has not been calibrated for both the CF and HF steel EHS under compression while the modified DSM [18] was calibrated against CF steel EHS stub columns only. In this study, the equivalent diameter method [8], the DSM [2] and the modified DSM [18] were used to calculate the nominal strengths of CF and HF steel elliptical tubular stub columns under compression.

The material properties obtained from the tensile coupon tests [17] at the flattest portion (R_{max}) of the section, namely, the location LT6 as shown in Figure 2, were used in the design strength calculation for conservative predictions. The $f_{0.2}$ and f_y as shown in Table 2 were used for CF and HF steel, respectively. Apart from the experimental and numerical results obtained from this study, the test results of CF steel [18, 22] and HF steel [8] EHS stub columns were also included in the comparison. Totally 57 and 84 results were used for the investigation of the CF and HF steel elliptical tubular stub columns, respectively.

The predictions of the three design methods were examined by reliability analysis. The reliability analysis that specified in the North American Specification AISI-S100 [2] was used. The reliability index (β) greater than or equal to 2.5 was set for the design provisions being considered reliable and probabilistically safe. The statistical parameters suggested in AISI-S100 [2] were used, where M_m = 1.10, F_m = 1.00, V_M = 0.10 and V_F = 0.05, which are the mean values and coefficients of variation of material factor and fabrication factor, respectively. The mean value (P_m) and the coefficients of variation (V_P) of tests (or FEA)-to-predicted strength ratio are shown in Tables 13-18. C_ϕ is the calibration coefficient associated to the design load combinations. The load combination of 1.35DL + 1.5LL was used for equivalent diameter method, while the load combination of 1.2DL + 1.6LL was used for the existing and modified DSM, where DL represents the dead load while LL represents the live load. The ratio of DL/LL is assumed to be 0.2. A correction factor (C_P) in the Section K2 of the AISI-S100 [2] was used in this study to take into consideration of the influence of limited number of test data, where $C_P = (1+1/n)m/(m-3)$, in which n is the number of tests and m ($m = n-1$) is the degrees of freedom. The resistance factors (ϕ_1) specified in the AISI-100 [2], and in the references [8, 18] were used. For the purpose of direct comparison, a constant resistance factor (ϕ_2) of 0.85 and a load combination of 1.2DL+1.6LL as specified in the AISI-100 [2] were used to calculate the reliability index (β_2), as shown in Table 18.

4.2. Equivalent diameter method

Chan and Gardner [8] conducted experimental and numerical investigations on HF steel EHS stub columns and developed the equivalent diameter method for the cross-section classification and design strength prediction of the EHS stub columns. The method was used for the cross-section classification in this study as mentioned earlier. The equivalent diameter ($D_e = 2a^2/b$) of EHS and the Class 3 slenderness limit of 90 proposed by Chan and Gardner [8] were adopted in this study. If the slenderness of EHS ($De/t\varepsilon^2$) is larger than 90, the EHS is classified as slender section and the effective area (A_{eff}) is calculated as per Eq. (1). Subsequently, the nominal stub column strength ($P_{C\&G}$) of EHS based on equivalent diameter method is calculated by Eq. (2). The applicability of the equivalent diameter method for the design of CF and HF steel elliptical tubular stub columns was assessed.

$$A_{eff} = A\left[\frac{90}{D_e/_t}\frac{235}{f_y}\right]^{0.5} \tag{1}$$

$$P_{C\&G} = \begin{cases} Af_y & \text{for } \frac{D_e}{t\varepsilon^2} \leq 90 \\ A_{eff}f_y & \text{for } \frac{D_e}{t\varepsilon^2} > 90 \end{cases} \tag{2}$$

4.3. Direct Strength Method

The Direct Strength Method (DSM) as detailed in Chapter E of the AISI-S100 [2] does not require the classification of section for the effectiveness of the cross-section area, whereas the full cross-section area is used in the calculation. The DSM can be used in predicting the strength of arbitrary cross-sections. However, the design equations of DSM were originally calibrated by open sections with plate elements. The applicability and reliability of the existing DSM for the design strength predictions of the EHS stub columns with curved cross-section profile should be evaluated.

In the DSM, the nominal axial strength (P_{DSM}) is determined by the minimum of the nominal axial strengths for flexural, torsional or flexural-torsional buckling as well as local buckling and distortional buckling. It should be noted that no distortional buckling and global buckling

was observed from the CF and HF steel elliptical tubular stub columns in the experimental and numerical studies. The calculation of elastic flexural buckling stress is detailed in Section E2.1 of the AISI-S100 [2]. The critical elastic local buckling load (P_{crl}) was obtained by the finite strip method suggested in the DSM. In this study, the CUFSM program [21] was used to calculate the critical elastic local buckling load of the CF and HF steel elliptical tubular stub columns. A 1.0 mm half-wavelength interval was used in the analysis by the CUFSM program [21]. The P_{DSM} can be obtained by substituting the resulted critical elastic local buckling load into the DSM design equations, as detailed in Section E3.2.1 of the AISI-S100 [2].

4.4. Modified Direct Strength Method

The DSM was modified by Chen and Young [18] by calibrating with the test and numerical strengths of CF steel elliptical tubular stub columns, as mentioned earlier. It should be noted that the modified DSM was calibrated for CF steel EHS stub columns only. Therefore, the applicability of the modified DSM for both CF and HF steel EHS stub columns should be further assessed in this study. In the modified DSM [18], the slenderness factor for local buckling (λ_l) is expressed by Eq. (3), and the nominal strength ($P_{C\&Y}$) is determined by the Eq. (4), where P_y ($P_y = Af_y$ or $P_y = Af_{0.2}$) is the squash load of the cross-section, where f_y and $f_{0.2}$ are the material properties at location LT6 of the cross-sections as mentioned previously. The modified DSM was simplified by considering the critical elastic local buckling load (P_{crl}) only since there is no distortional buckling observed in the experimental and numerical studies.

$$\lambda_l = \sqrt{\frac{P_y}{P_{crl}}} \tag{3}$$

$$P_{C\&Y} = \begin{cases} 1.2P_y & \text{for } \lambda_l \leq 0.178 \\ \left[1 - 0.16\left(\frac{P_{crl}}{P_y}\right)^{0.14}\right]\left(\frac{P_{crl}}{P_y}\right)^{0.14} P_y & \text{for } \lambda_l > 0.178 \end{cases} \tag{4}$$

4.5. Comparisons and discussions

Table 13-17 illustrates the comparison between the numerical strengths (P_{FEA}) and the predicted strengths ($P_{C\&G}$, P_{DSM} and $P_{C\&Y}$) for both the CF and HF steel elliptical tubular stub

columns. The stub columns in Tables 13-17 are corresponding to those of Tables 8-12 designed in the parametric study. Overall, it is found that the predictions of $P_{C\&G}$, P_{DSM} and $P_{C\&Y}$ are all conservative both CF and HF EHS as the values of $P_{FEA}/P_{C\&G}$, P_{FEA}/P_{DSM} and $P_{FEA}/P_{C\&Y}$ are greater than 1.0, as shown in Table 13-17.

The mean values (P_m) of $P_{FEA}/P_{C\&G}$ and P_{FEA}/P_{DSM} for both CF and HF steel stub columns with Class 1-3 EHS are similar, e.g., same value of 1.43 for Class 1, with the similar V_P of 0.084 and 0.085 as shown in Table 13. The mean values of P_{FEA}/P_{DSM} is smaller than that of $P_{FEA}/P_{C\&G}$ for CF and HF steel stub columns with Class 4 section, e.g., P_m=1.35 for P_{FEA}/P_{DSM} and P_m=1.23 for $P_{FEA}/P_{C\&G}$ for HF steel as shown in Table 16, which means that the DSM provides better predictions for CF and HF steel EHS stub columns with slender cross-section. It is shown that both the P_m and V_P of $P_{FEA}/P_{C\&Y}$ are always smaller than those of $P_{FEA}/P_{C\&G}$ and P_{FEA}/P_{DSM} for both CF and HF steel stub columns regardless of the section slenderness limit, as shown in Tables 13-17. It means that the modified DSM proposed by Chen and Young [18] provides better strength predictions than the equivalent diameter method proposed by Chan and Gardner [8] as well as the DSM specified in AISI-S100 [2].

The predictions of $P_{C\&G}$, P_{DSM} and $P_{C\&Y}$ were further assessed using not only the experimental and numerical results of CF and HF steel elliptical tubular stub columns obtained from this study, but also the test results of CF steel [18, 22] and HF steel [8] EHS stub columns in the literature. The reliability of the predictions was also assessed by reliability analysis. Figures 16-17 present the comparison of the strengths (P_u) obtained from the tests (P_t) and FEA (P_{FEA}) with those of the predictions for $P_{C\&G}$, P_{DSM} and $P_{C\&Y}$, respectively. Figure 16 plots the strength ratio $P_u/P_{C\&G}$ against the value of cross-section slenderness ($De/t\varepsilon^2$) for the equivalent diameter method. Figures 17(a)-(b) plot the strength ratio against the slenderness factor for local buckling (λ_l) proposed in [18] for the purpose of direct comparison between the DSM [2] and the modified DSM [18]. A total of 57 and 84 results were used for the CF and HF steel elliptical tubular stub columns, respectively, as shown in Table 18. For the CF stub columns, the mean value of $P_u/P_{C\&G}$, P_u/P_{DSM} and $P_u/P_{C\&Y}$ are 1.32, 1.24 and 1.12, respectively, with the corresponding V_P of 0.105, 0.111 and 0.092. For HF stub columns, the mean value of $P_u/P_{C\&G}$, P_u/P_{DSM} and $P_u/P_{C\&Y}$ are 1.30, 1.17 and 1.06 with V_P of 0.128, 0.138 and 0.105, respectively. Overall, the predictions of $P_{C\&G}$, P_{DSM} and $P_{C\&Y}$ are conservative, among which the predictions of $P_{C\&Y}$ [18] are more accurate with smaller V_P than those of $P_{C\&G}$ and P_{DSM} for both CF and HF steel EHS stub columns. The predictions of P_{DSM} [2] are

less conservative than those of $P_{C\&G}$ but with larger values of V_P for both CF and HF steel EHS stub columns. The reliability indices are greater than 2.5 for all the three predictions of $P_{C\&G}$, P_{DSM} and $P_{C\&Y}$, although the values of β_2 are smaller for $P_{C\&Y}$ compared with those of $P_{C\&G}$ and P_{DSM} under the same value of ϕ_2. Therefore, it could be concluded that the modified DSM proposed by Chen and Young [18] provides more accurate and reliable predictions than the equivalent diameter method [8] and DSM [2] for both CF and HF steel elliptical tubular stub columns.

5. Conclusions

Behavior of cold-formed (CF) and hot-finished (HF) steel elliptical tubular stub columns has been presented. Experimental investigation, including initial local imperfection measurements and stub column tests, on the CF and HF steel elliptical tubular stub columns was conducted. In addition, non-linear finite element model was developed and a series of sensitive analyses on the effect of parameters on the ultimate strength of the CF and HF steel elliptical tubular stub columns was performed. The model was validated against the test results obtained from this study and also from the literature. By using the validated finite element model, an extensive parametric study was performed, which covered broad range of cross-section slenderness and aspect ratios of CF and HF steel elliptical tubular stub columns. The parameters were carefully designed such that the cold-forming effects on the CF stub columns were considered in a conservative manner.

The experimentally and numerically obtained CF and HF steel stub column strengths were compared with the design strengths predicted by the equivalent diameter method [8], the Direct Strength Method (DSM) [2] and the modified DSM [18]. The existing test results of CF and HF steel elliptical tubular stub columns reported in the existing literature were also included in the comparison. Totally 57 and 84 results were used for the CF and HF steel elliptical tubular stub columns, respectively. It is found that the equivalent diameter method, the DSM and the modified DSM generally provide conservative design strength predictions for both CF and HF steel elliptical hollow section (EHS) stub columns. The results of reliability analysis indicated that the predictions by the three design methods are all reliable for both the CF and HF steel elliptical tubular stub columns. Among these three design methods, the modified DSM provides the most accurate and the least scattered predictions. Therefore, the modified DSM is recommended for the design of CF and HF steel elliptical

tubular stub columns.

Acknowledgements

The authors are grateful to Wo Lee Steel Co. Ltd. Hong Kong for supplying the cold-formed and hot-finished elliptical hollow section test specimens. The research work described in this paper was supported by grants from the Fundo para o Desenvolvimento das Ciências e da Tecnologia (FDCT) of the Macao S.A.R. (Project No. 129/2014/A3) and the Research Grants Council of the Hong Kong Special Administrative Region, China (Project No. 17267416).

References

[1] J.A. Packer. Going elliptical, Modern Steel Construction. March, 2008,

[2] AISI-S100. North American Specification for the design of cold-formed steel structural members. AISI S100-16. Washington,D.C., USA: American Iron and Steel Institute, 2016.

[3] ANSI/AISC 360. Specification for Structural Steel Buildings. ANSI/AISC 360-16. Chicago, IL, USA: American Institute of Steel Construction, 2016.

[4] AS4100. Steel structures. AS 4100: Homebush, New South Wales, Australia: Standards Australia, 1998.

[5] AS/NZS4600. Cold-formed steel structure. AS/NZS 4600: 2018. Sydney: Standards Australia/Standards New Zealand, 2018.

[6] EC3-1.1. Eurocode 3–Design of steel structures–Part 1.1: General rules and rules for buildings. EN 1993-1-1:2005. Brussels, Belgium: European Committee for Standardization.

[7] EC3-1.3. Eurocode 3–Design of Steel Structures–Part 1-3: General Rules Supplementary Rules for Cold-formed Members and Sheeting, EN 1993-1-3:2006. Brussels, Belgium European Committee for Standardization,

[8] T.M. Chan and L. Gardner. Compressive resistance of hot rolled elliptical hollow sections, Engineering Structures 30(2): 522–532, 2008.

[9] T.M. Chan and L. Gardner. Bending strength of hot-rolled elliptical hollow sections, Journal of Constructional Steel Research, 64(9): 971–986, 2008.

[10] L. Gardner, T.M. Chan and M.A. Wadee. Shear response of elliptical hollow sections, Proceedings of the Institution of Civil Engineers, Structures and Buildings, 161(6): 301–309, 2008.

[11] T.M. Chan and L. Gardner. Flexural buckling of elliptical hollow section columns ASCE

Journal of Structural Engineering, 135(5): 546–557, 2009.
[12] K.H. Law and L. Gardner. Buckling of elliptical hollow section members under combined compression and uniaxial bending, Journal of Constructional Steel Research, 86:1-16, 2013.
[13] E. Bortolotti, J.P. Jaspart, C. Pietrapertosa, G. Nicaud, P.D. Petitjean and J.P. Grimault. Testing and modelling of welded joints between elliptical hollow sections, Proceedings of the 10th International Symposium on Tubular Structures, Madrid. Taylor & Francis, London, pp. 259–266, 2003.
[14] C. Pietrapertosa and J.P. Jaspart. Study of the behaviour of welded joints composed of elliptical hollow sections, Proceedings of the 10th International Symposium on Tubular Structures, Madrid. Taylor & Francis, London, pp. 601–608, 2003.
[15] S. Willibald, J.A. Packer, A.P. Voth and X. Zhao. Through plate joints to elliptical and circular hollow sections, Proceedings of the 11th International Symposium on Tubular Structures, Quebec City. Taylor & Francis, London, pp. 221–228, 2006.
[16] S. Willibald, J.A. Packer and G. Martinez-Saucedo. Behaviour of gusset plate connections to ends of round and elliptical hollow structural section members, Canadian Journal of Civil Engineering, 33(4): 373–383, 2006.
[17] W. M. Quach and B. Young. Material properties of cold-formed and hot-finished elliptical hollow sections, Advances in Structural Engineering, 18(7), 1101-1114, 2014.
[18] M.T. Chen and B. Young. Material properties and structural behavior of cold-formed steel elliptical hollow section stub columns. Thin-Walled Structures, 134: 111–126, 2019.
[19] M.T. Chen and B. Young. Cross-sectional behavior of cold-formed steel semi-oval hollow sections. Engineering Structures, 177: 318–330, 2018.
[20] M.T. Chen and B. Young. Experimental and numerical investigation on cold-formed steel semi-oval hollow section compression members. Journal of Constructional Steel Research, 151: 174–184, 2018.
[21] B.W. Schafer and S. Ádány Buckling analysis of cold-formed steel members using CUFSM: conventional and constrained finite strip methods. in: Proceedings of the Eighteenth International Specialty Conference on Cold-Formed Steel Structures, Orlando, FL, USA, 2006. pp. 39–54.
[22] T.M. Chan, Y.M. Huai and W. Wang, Experimental investigation on lightweight concrete-filled cold-formed elliptical hollow section stub columns, J. Constr. Steel Res. 115:434–444, 2015.

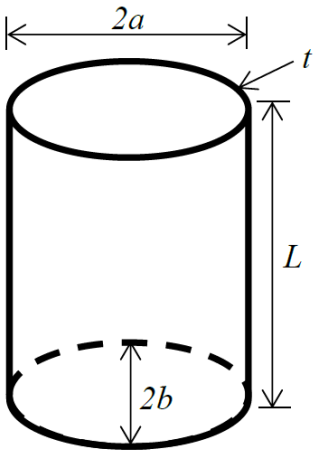

(a) 3-D view

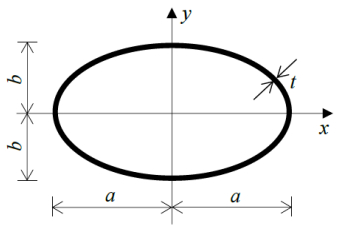

(b) Plan view

Figure 1: Configuration of steel elliptical tubular stub column

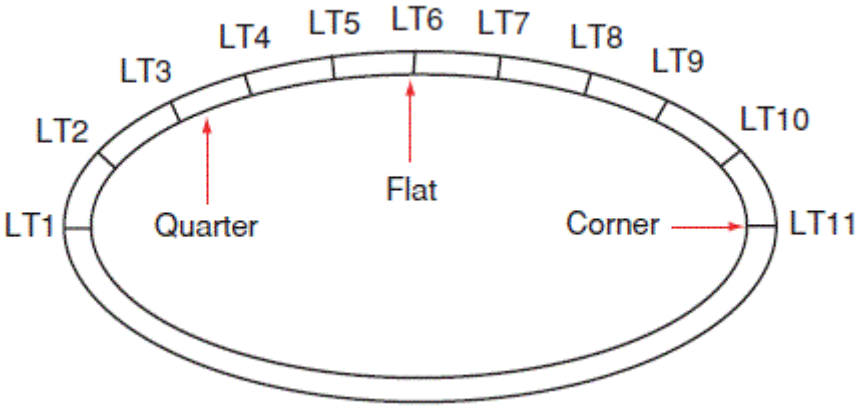

Figure 2: Tensile coupon specimens tested across the section [17]

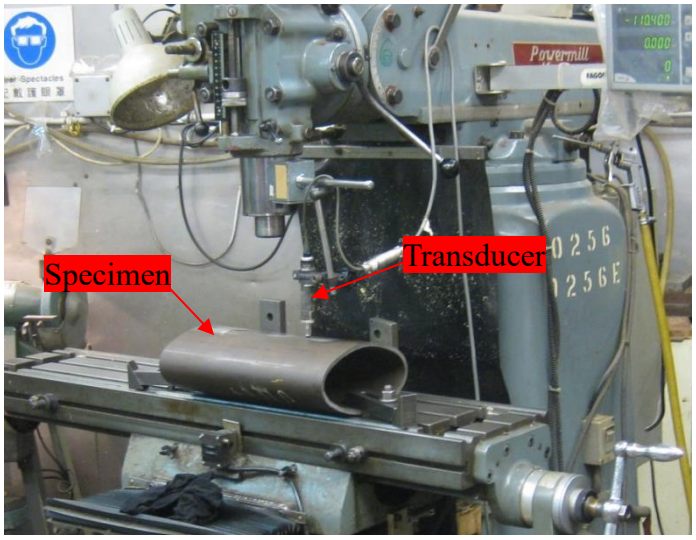

Figure 3: Setup of imperfection measurement for Specimen CF-SC

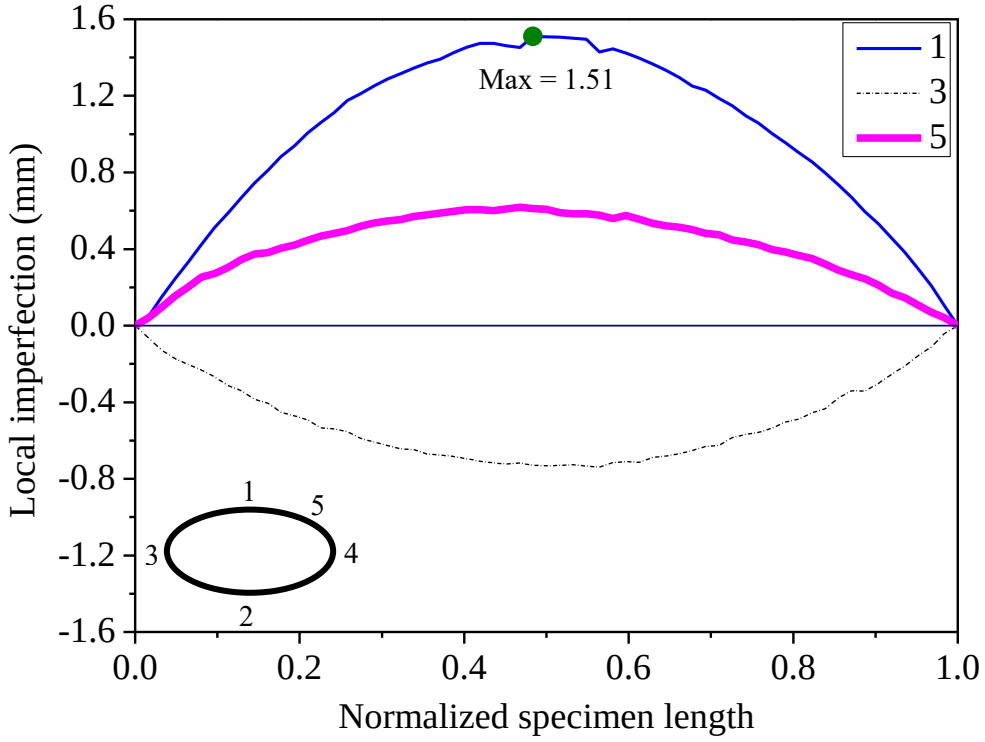

(a) Specimen CF-SC

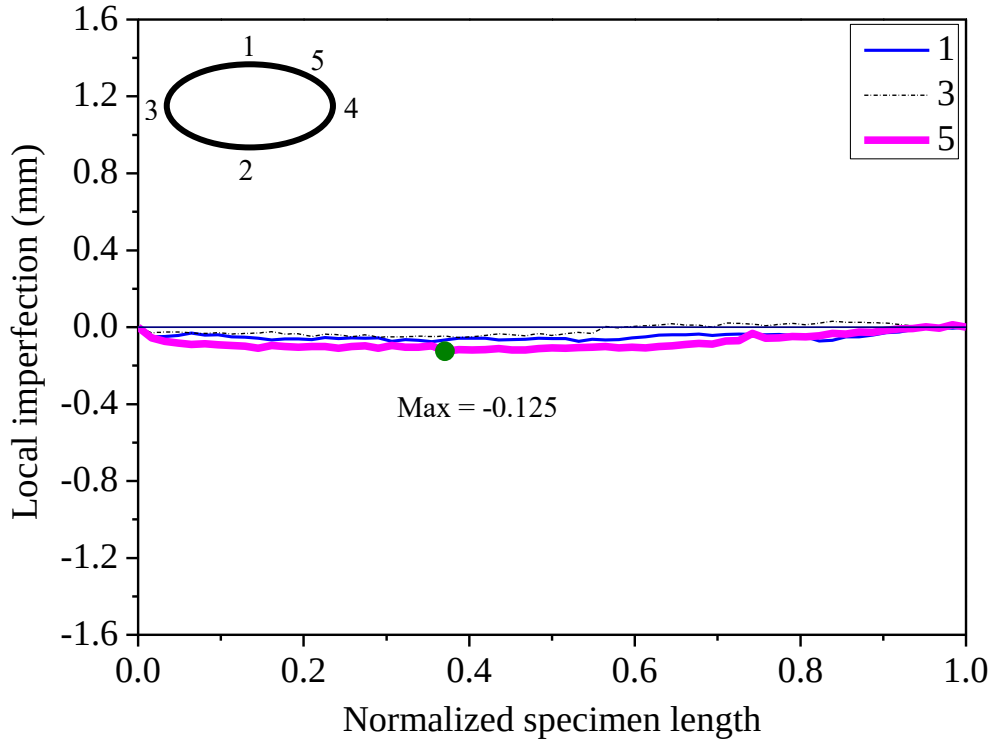

(b) Specimen HF-SC

Figure 4: Measured local imperfection profiles for stub column specimens

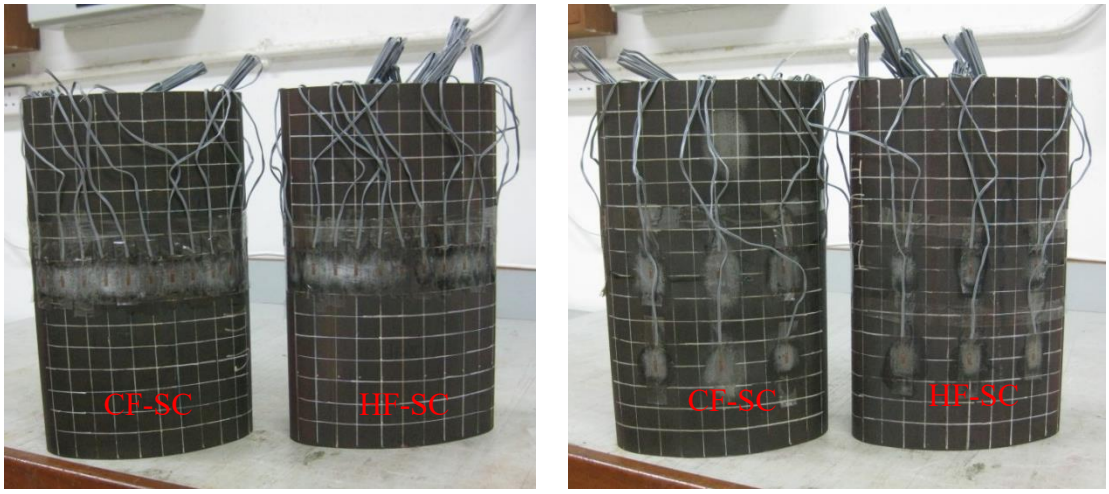

(a) Strain gauges No. 1 to No. 13 (b) Strain gauges No. 14 to No. 19

Figure 5: Arrangement of strain gauges of the stub column specimens

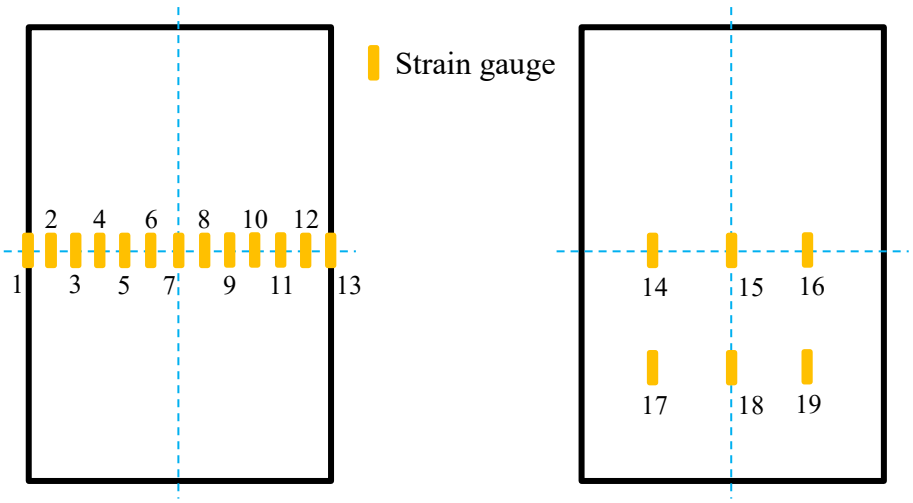

Figure 6: Numbering of strain gauges of the stub column specimens

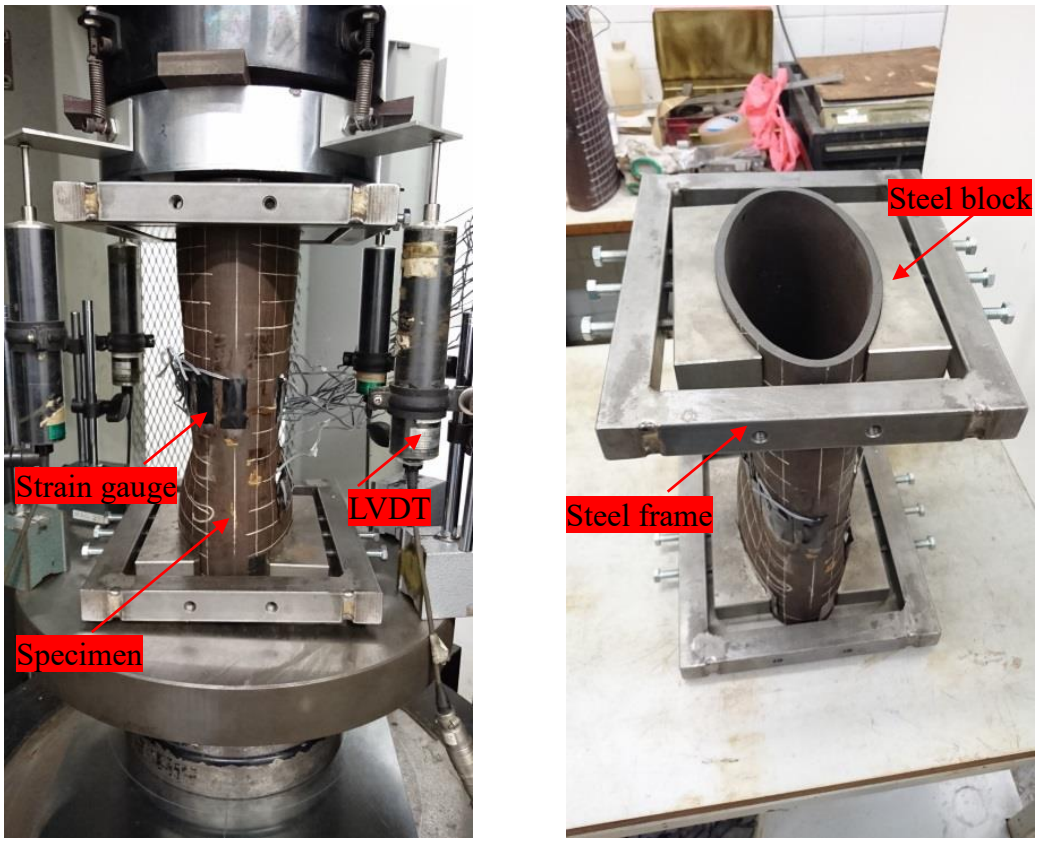

Figure 7: Specimen HF-SC during testing (left) and after testing (right)

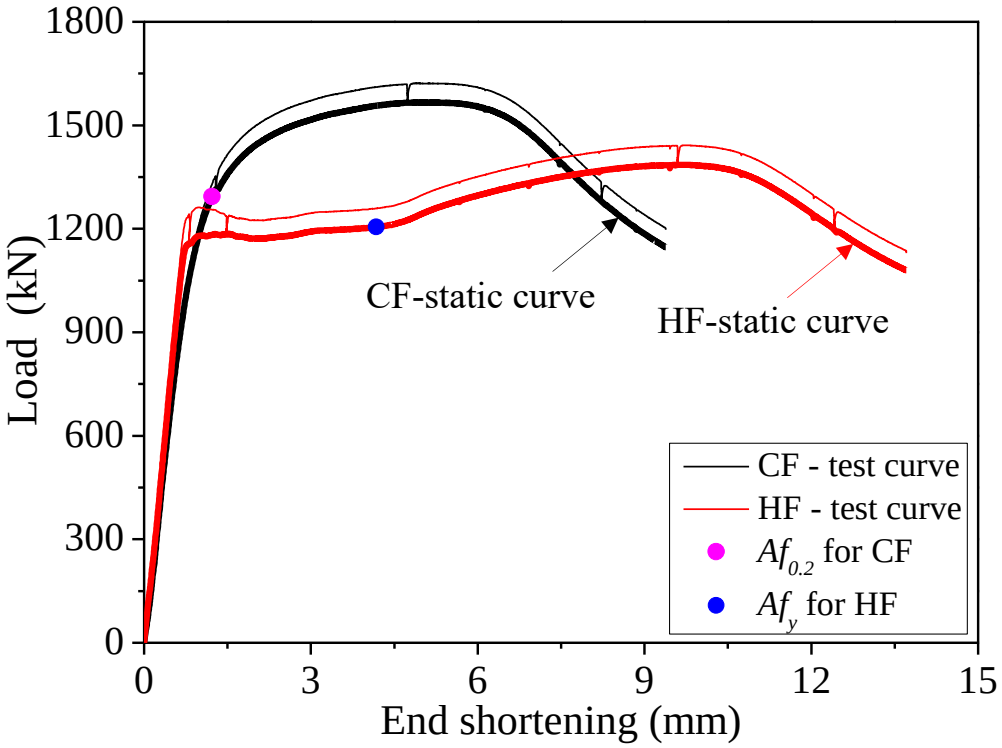

Figure 8: Load-end shortening of EHS stub columns

(a) Specimen CF-SC (b) Specimen HF-SC (c) FEA of CF-SC

Figure 9: Failure mode of EHS stub columns

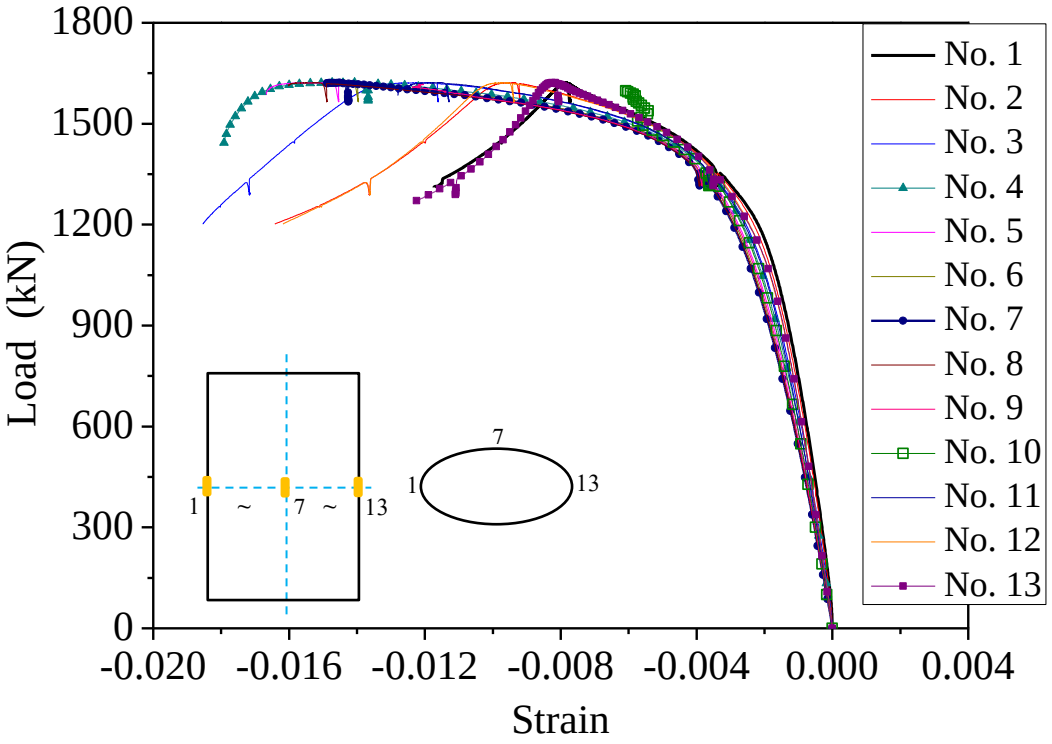

(a) Specimen CF-SC

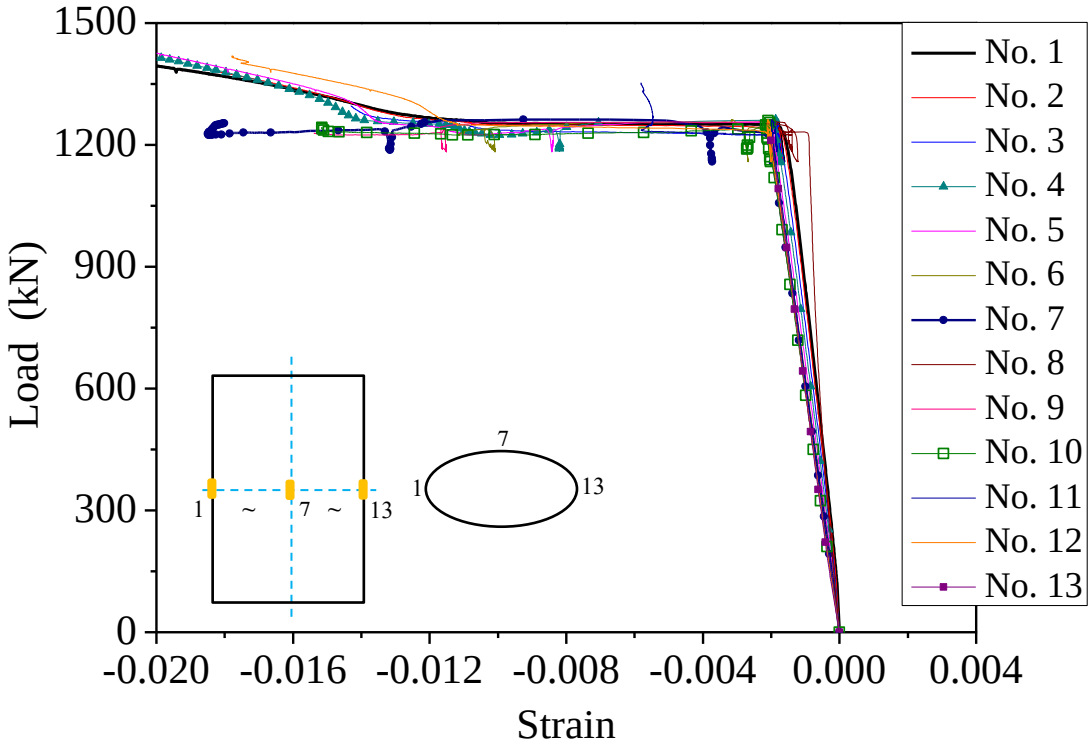

(b) Specimen HF-SC

Figure 10: Complete load-strain curves with strain readings obtained from strain gauges No.1 to No. 13

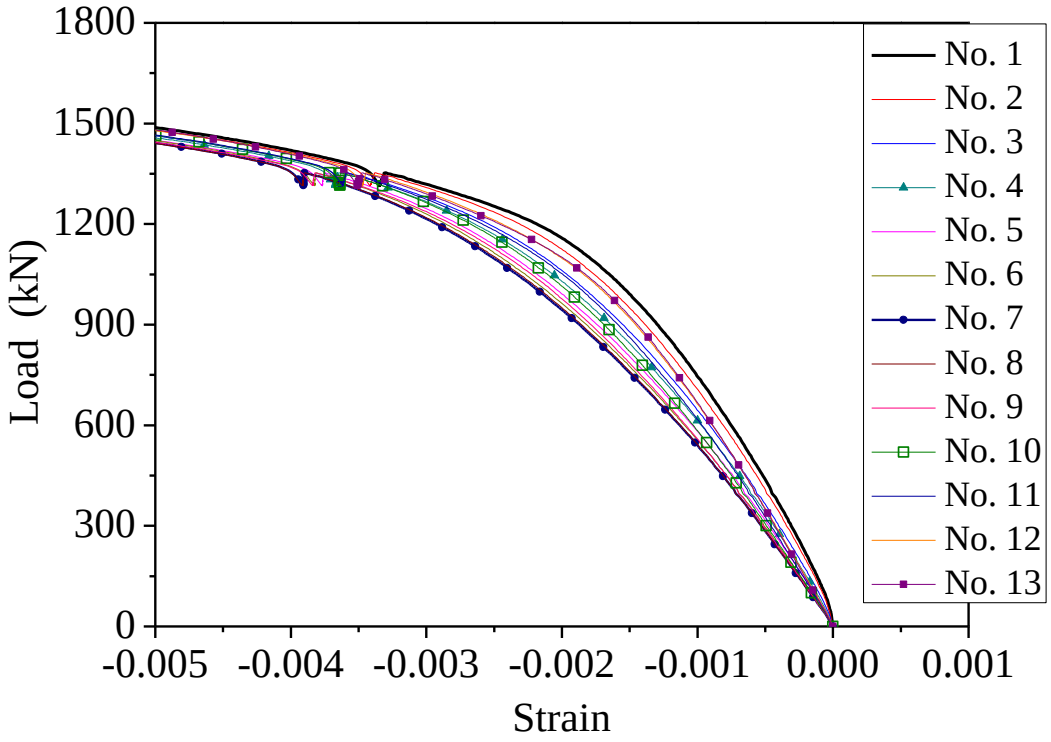

(a) Specimen CF-SC

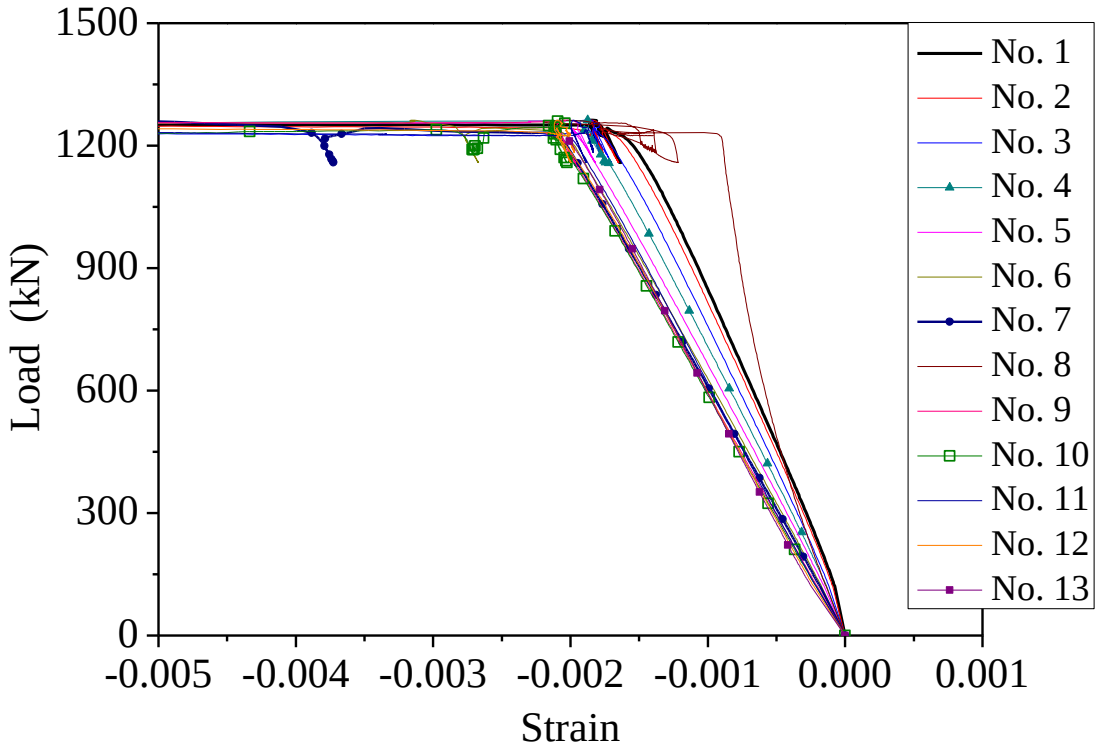

(b) Specimen HF-SC

Figure 11: Initial part of load-strain curves with strain readings obtained from strain gauges No.1 to No. 13

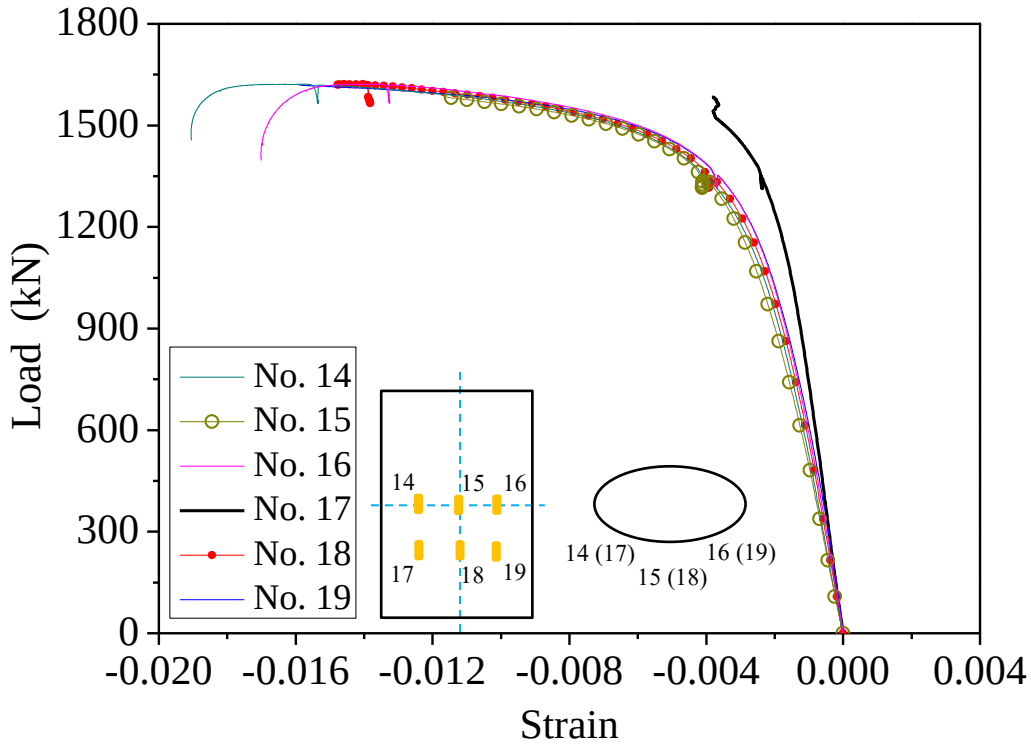

(a) Specimen CF-SC

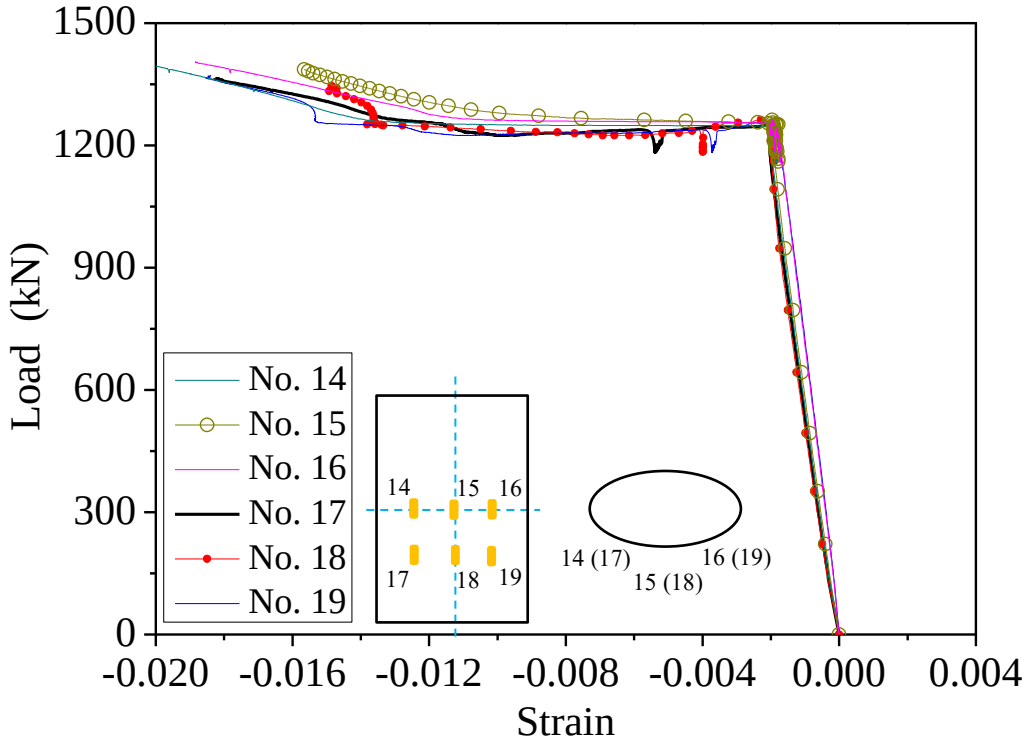

(b) Specimen HF-SC

Figure 12: Complete load-strain curves with strain readings obtained from strain gauges No.14 to No. 19

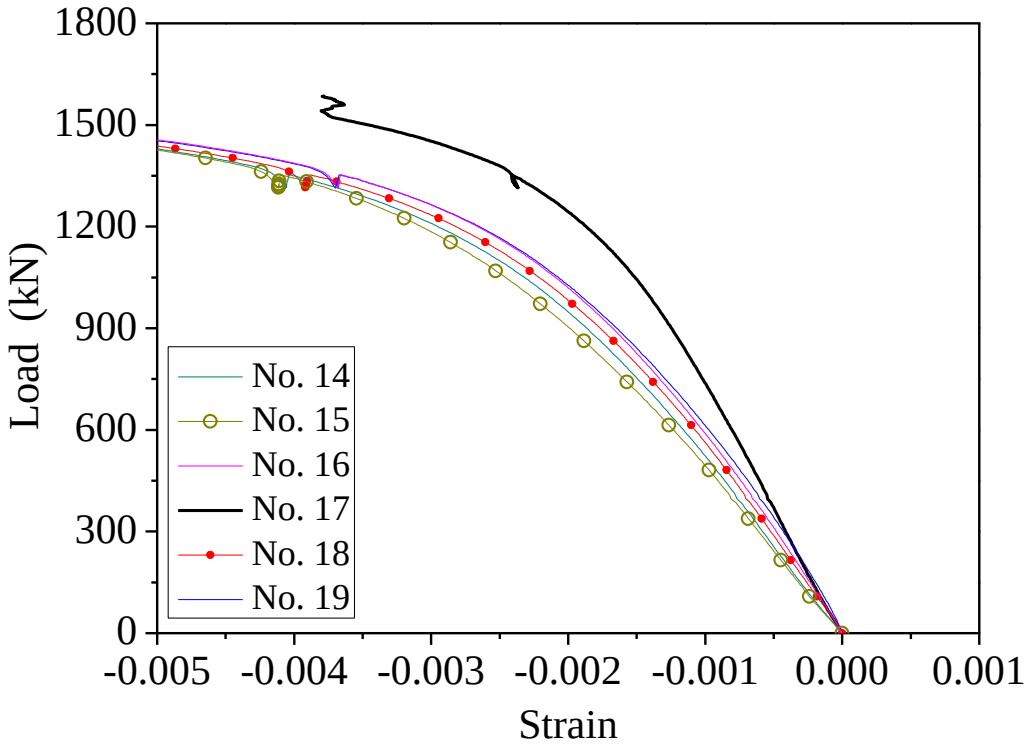

(a) Specimen CF-SC

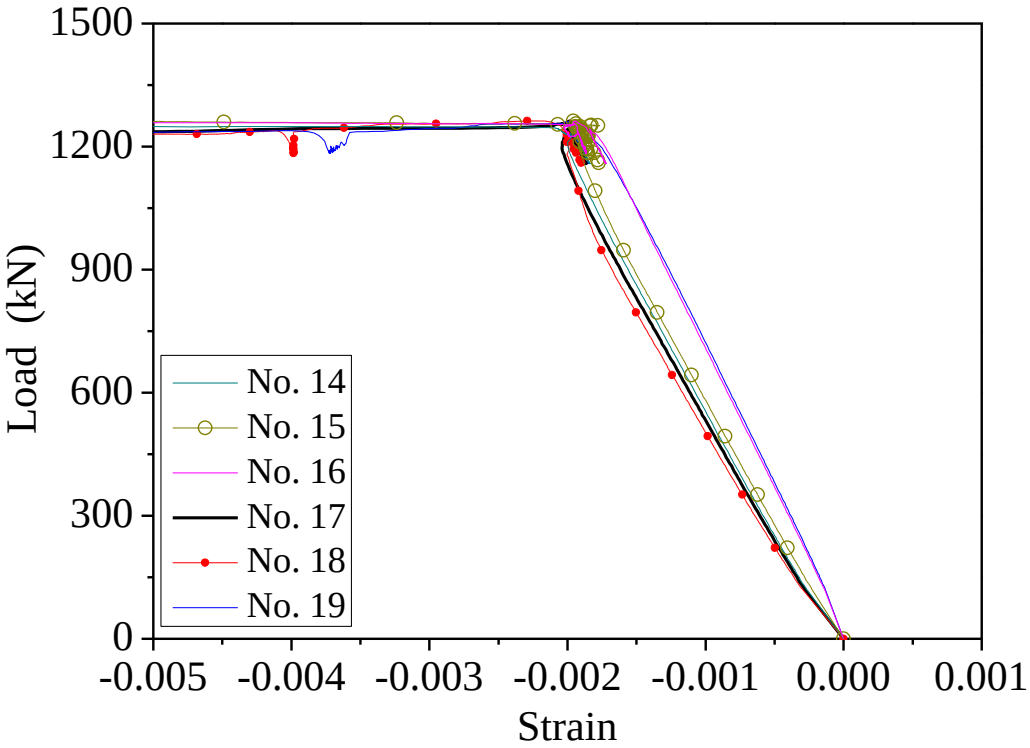

(b) Specimen HF-SC

Figure 13: Initial part of load-strain curves with strain readings obtained from strain gauges No.14 to No. 19

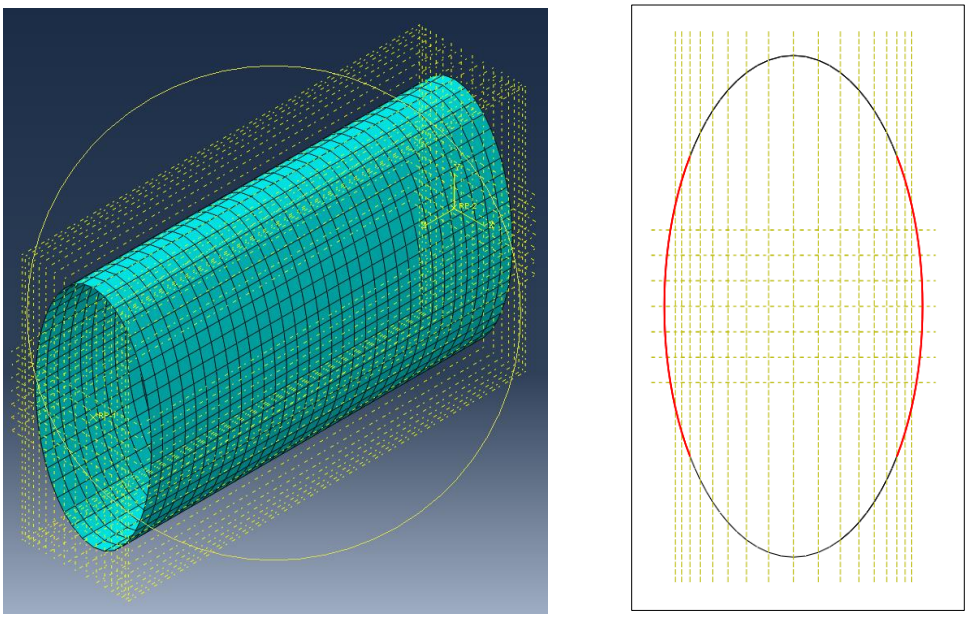

(a) Meshed with element size of 10×10mm (b) Section portioned

Figure 14: Finite element model of EHS stub column with section portioned

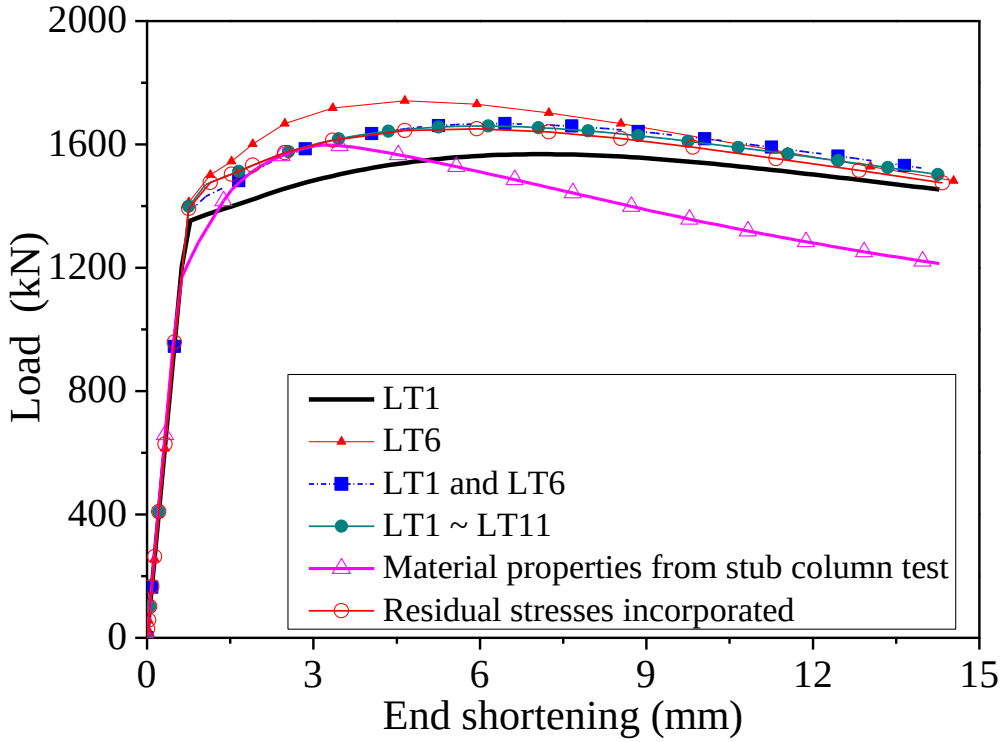

(a) Specimen CF-SC

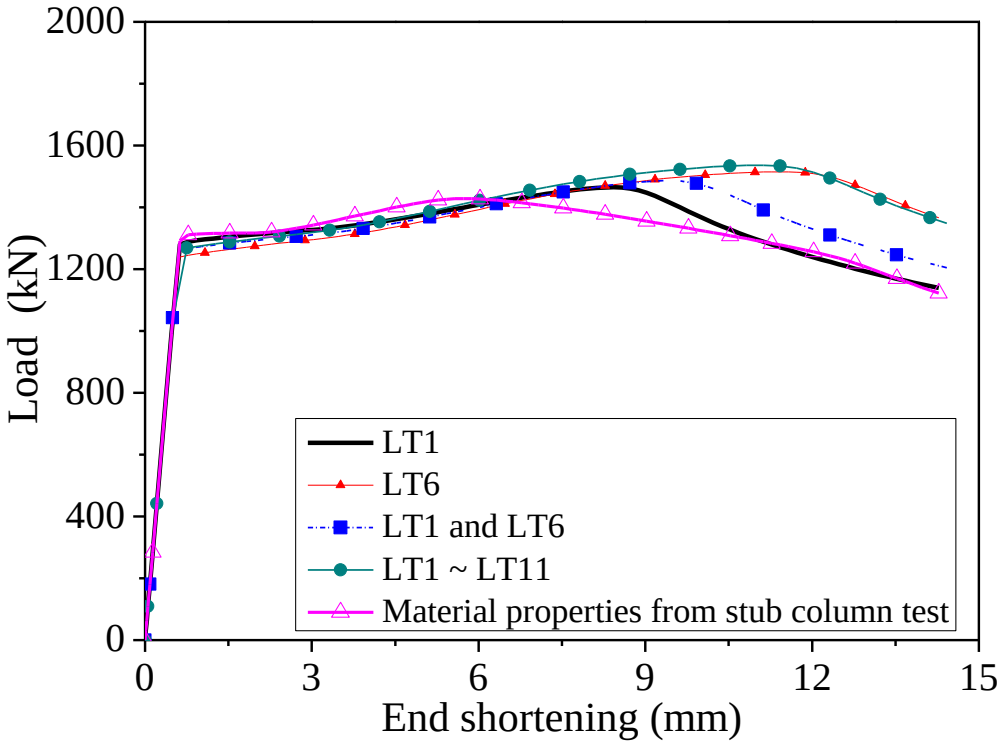

(b) Specimen HF-SC

Figure 15: Effects of material properties inputs on the load-end shortening curves from FEA

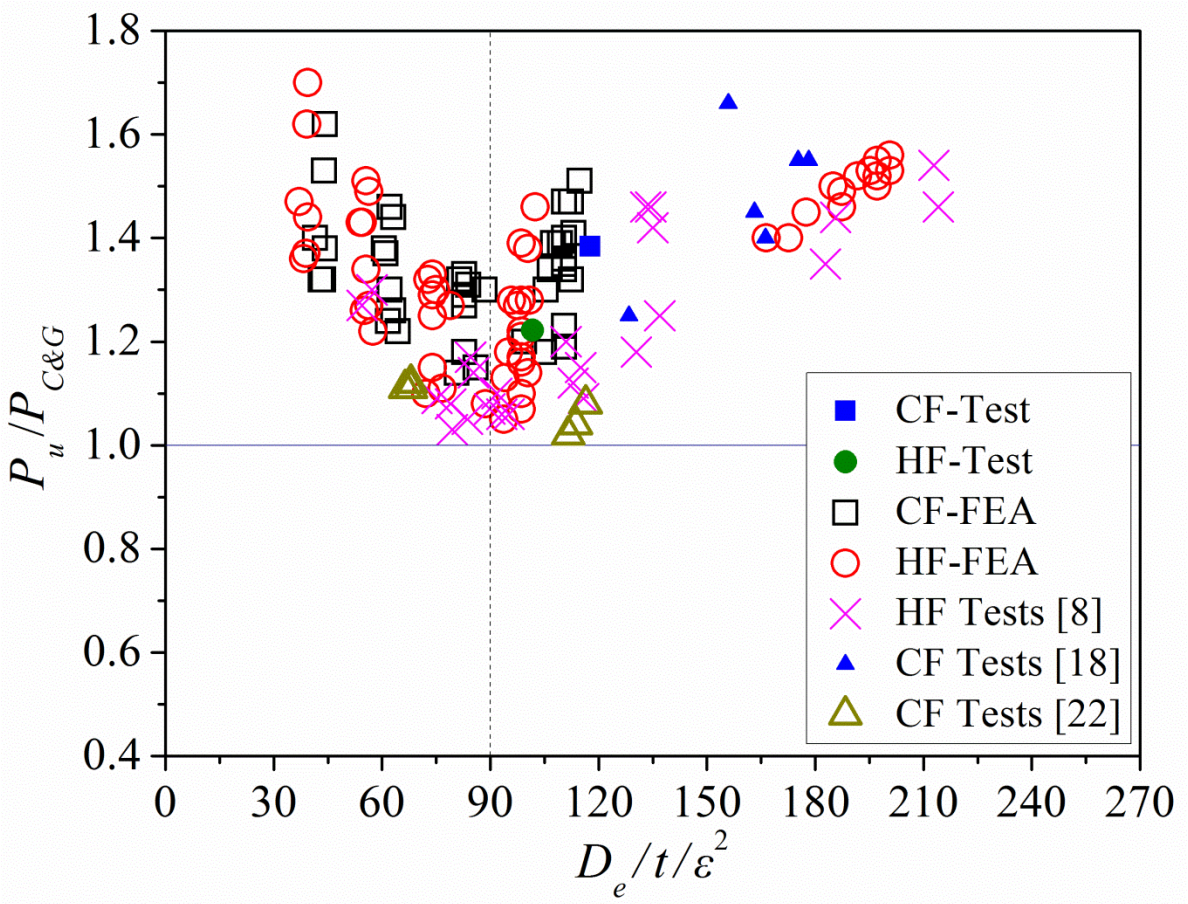

Figure 16: Comparison of test and FE results with design strengths predicted by Chan and Gardner [8]

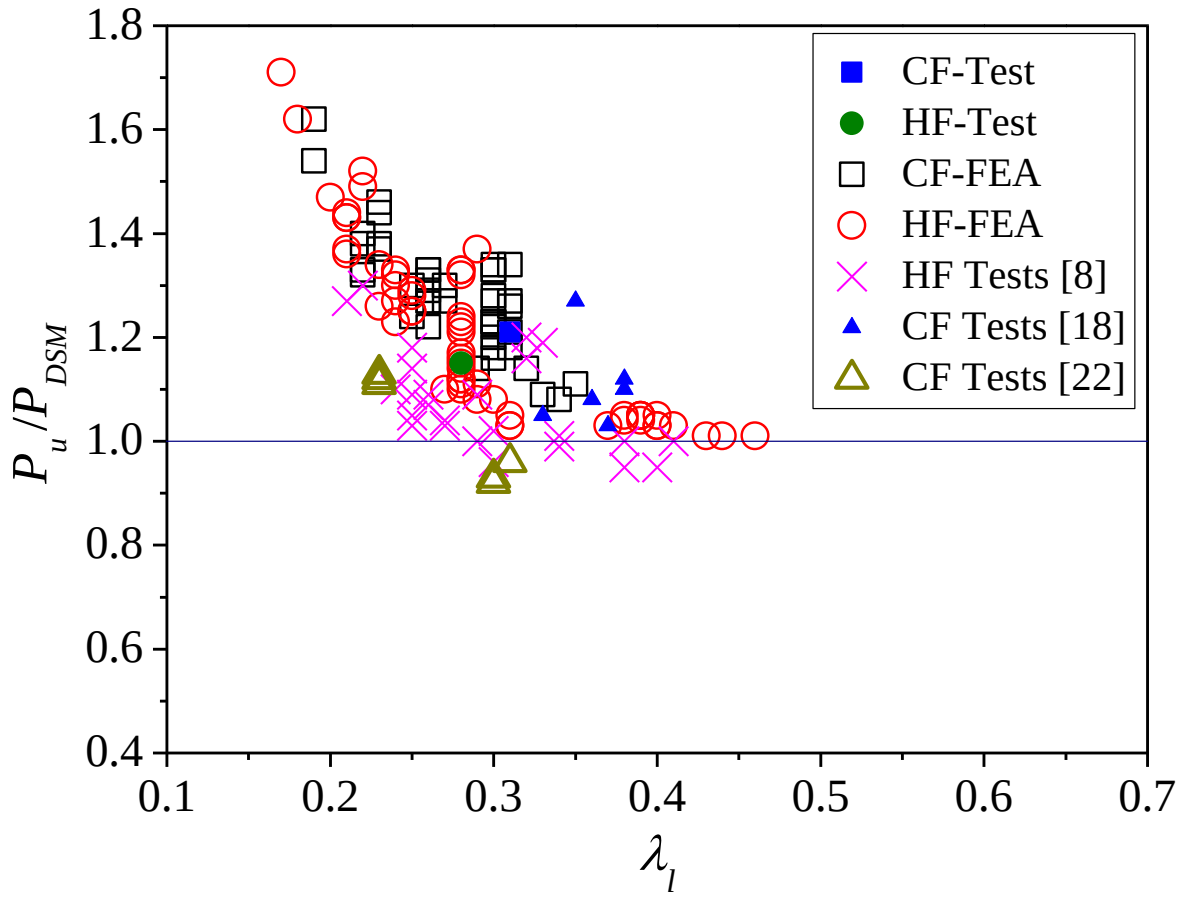

(a) Predicted by DSM [2]

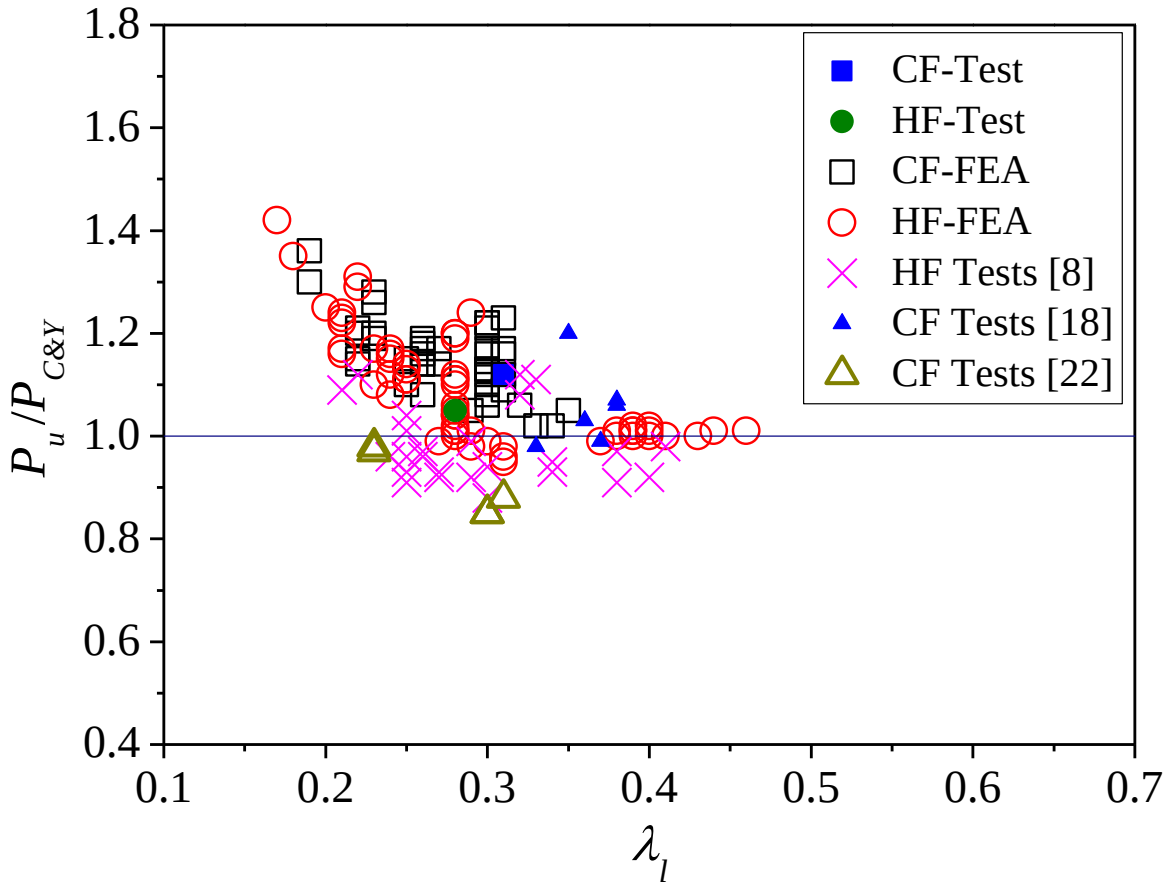

(b) Predicted by modified DSM by Chen and Young [18]

Figure 17: Comparison of test and FE results with DSM predictions

Table 1: Measured dimensions of EHS stub columns

Labeling	$2a$ (mm)	$2b$ (mm)	t (mm)	L (mm)	w_o (mm)	A (mm^2)	R_{max}	R_{min}	R_{max}/t	R_{min}/t
CF-SC	204.9	105.9	6.22	331.2	1.510	2990.9	198.2	27.4	32.0	4.4
HF-SC	204.3	102.9	6.56	330.4	0.125	3120.7	202.8	25.9	30.7	3.9

Table 2: Static material properties of EHS from tensile coupon tests [17]

Labeling	Location	E (GPa)	$f_{0.2}$ (MPa)	f_y (MPa)	f_u (MPa)	ε_u (%)	ε_f (%)
CF	Flattest (LT6)	201.1	432.6	-	571.9	11.6	29.9
	Curviest (LT1)	196.6	465.4		589.0	7.3	25.8
	Mean	201.1	462.3	-	575.9	9.3	27.1
HF	Flattest (LT6)	206.8	387.1	386.2	533.6	13.8	30.9
	Curviest (LT1)	209.0	374.4	373.2	530.5	13.2	31.0
	Mean	206.3	382.3	383.2	537.6	12.4	30.8

Table 3: Test results of EHS stub columns

Labeling	P_t* (kN)	P_t (kN)	δ_u (mm)	$P_t/Af_{0.2}$ or P_t/Af_y	
				Using LT1	Using LT6
CF-SC	1622.1	1566.7	4.9	1.13	1.21
HF-SC	1442.3	1385.7	9.7	1.19	1.15

Table 4: Static material properties of EHS from stub column tests

Labeling	Strain gauge	E (GPa)	$f_{0.2}$ (MPa)	f_y (MPa)
CF-SC	No. 3	211.0	453.0	-
HF-SC	No. 13	206.7	400.0	400.0

Table 5: Summary of sensitivity analysis by comparing with the test results

Material properties	CF-SC			HF-SC		
	w (mm)	P_{FEA} (kN)	P_t/P_{FEA}	w (mm)	P_{FEA} (kN)	P_t/P_{FEA}
Case 1	1.51	1362.2	1.15	0.125	1413.1	0.98
	t/10	1457.4	1.08	t/10	1304.2	1.06
	t/50	1571.4	1.00	t/50	1409.5	0.98
	t/100	1568.3	1.00	t/100	1465.1	0.95
Case 2	1.51	1544.5	1.01	0.125	1452.8	0.95
	t/10	1658.1	0.95	t/10	1281.9	1.08
	t/100	1741.7	0.90	t/100	1515.1	0.92
Case 3	1.51	1446.3	1.08	0.125	1422.3	0.97
	t/10	1572.2	1.00	t/10	1288.1	1.08
	t/100	1667.3	0.94	t/100	1486.2	0.93
Case 4	1.51	1467.0	1.07	0.125	1474.9	0.94
	t/10	1566.7	1.00	t/10	1305.0	1.06
	t/100	1659.2	0.94	t/100	1536.2	0.90
Case 5	1.51	1462.1	1.07	0.125	1419.4	0.98
	t/10	1557.8	1.01	t/10	1326.0	1.05
	t/100	1598.1	0.98	t/100	1428.6	0.97
Case 6	1.51	1466.7	1.07			
	t/10	1554.6	1.01			
	t/100	1651.1	0.95			

Table 6: Verification of the developed finite element model for parametric study

Specimens	P_t (kN)	P_{FEA} (kN)	P_t/P_{FEA}
CF-SC	1566.7	1571.4	1.00
140×85×3-SCL350*	422.5	414.8	1.02
150×50×5-SCL375*	819.7	710.7	1.15
150×70×3-SCL375*	351.8	325.5	1.08
150×70×3-SCL375-r*	330.5	318.9	1.04
180×65×5-SCL450*	863.2	786.5	1.10
180×65×5-SCL270-r*	854.0	787.1	1.09
HF-SC	1385.7	1409.5	0.98
150×75×4-SC1#	538	562.8	0.96
150×75×5-SC1#	689	679.2	1.01
150×75×6.3-SC1#	896	896.6	1.00
150×5×8.0-SC1#	1367	1422.9	0.96
300×150×8.0-SC1#	2777	2319.3	1.20
400×200×8.0-SC1#	2961	3123.5	0.95
400×200×10.0-SC1#	3521	3579.8	0.98
400×200×12.5-SC1#	4727	4380.8	1.08
400×200×14.0-SC1#	5610	5452.9	1.03
400×200×16.0-SC1#	6310	5978.2	1.06
500×250×8.0-SC1#	3684	3662.0	1.01
		Mean	1.04
		COV	0.064

Note: * indicates the test results from [18], # indicates the test results from [8].

Table 7: Parameters design for CF and HF EHS stub columns

Section slenderness	*2a* (mm)	*t* (mm)	*a/b*	Number	
				CF	HF
Class 1	120, 270, 420, 570	5.0 ~ 24.0	1.0, 1.5, 2.0	6	6
Class 2		3.5 ~ 26.0	1.0, 1.5, 2.0	8	8
Class 3		4.0 ~ 25.0	1.0, 1.5, 2.0	10	10
Class 4		1.0 ~ 28.0	1.0, 1.5, 2.0, 2.5, 3.0	20	34
			Total	44	58

Table 8: Dimensions of CF and HF EHS stub columns with Class 1 cross-section ($D_e/t\varepsilon^2 \leq 50$)

Labeling	*2a* (mm)	*t* (mm)	*a/b*	*A* (mm^2)	R_{max}/t	$D_e/t\varepsilon^2$	
						CF	HF
120×120×5	120.0	5.0	1.0	1806	12.0	44.2	39.4
120×60×10	120.0	10.0	2.0	2602	12.0	44.2	39.4
270×270×12	270.0	12.0	1.0	9726	11.3	41.4	37.0
270×180×17	270.0	17.0	1.5	11239	11.9	43.9	39.2
420×420×18	420.0	18.0	1.0	22733	11.7	43.0	38.3
570×570×24	570.0	24.0	1.0	41167	11.9	43.7	39.0

Table 9: Dimensions of CF and HF EHS stub columns with Class 2 cross-section ($50 < D_e/t\varepsilon^2 \leq 70$)

Labeling	*2a* (mm)	*t* (mm)	*a/b*	*A* (mm^2)	R_{max}/t	$D_e/t\varepsilon^2$	
						CF	HF
120×120×3.5	120.0	3.5	1.0	1281	17.1	63.1	56.3
120×60×7	120.0	7.0	2.0	1885	17.1	63.1	56.3
270×270×8	270.0	8.0	1.0	6585	16.9	62.1	55.5
270×135×16	270.0	16.0	2.0	9684	16.9	62.1	55.5
420×420×12	420.0	12.0	1.0	15381	17.5	64.4	57.5
420×280×19	420.0	19.0	1.5	19979	16.6	61.0	54.5
570×570×17	570.0	17.0	1.0	29534	16.8	61.7	55.1
570×380×26	570.0	26.0	1.5	37087	16.4	60.5	54.0

Table 10: Dimensions of CF and HF EHS stub columns with Class 3 cross-section ($70 < D_e/t\varepsilon^2 \leq 90$)

Labeling	*2a* (mm)	*t* (mm)	*a/b*	*A* (mm^2)	R_{max}/t	$D_e/t\varepsilon^2$	
						CF	HF
120×80×4	120.0	4.0	1.5	1219	22.5	82.8	74.0
120×60×5	120.0	5.0	2.0	1377	24.0	88.4	78.9
270×270×6	270.0	6.0	1.0	4976	22.5	82.8	74.0
270×135×12	270.0	12.0	2.0	7409	22.5	82.8	74.0
420×420×9	420.0	9.0	1.0	11621	23.3	85.9	76.7
420×280×14	420.0	14.0	1.5	14939	22.5	82.8	74.0
420×210×19	420.0	19.0	2.0	18229	22.1	81.4	72.7
570×570×13	570.0	13.0	1.0	22748	21.9	80.7	72.1
570×380×19	570.0	19.0	1.5	27515	22.5	82.8	74.0
570×285×25	570.0	25.0	2.0	32611	22.8	83.9	74.9

Table 11: Dimensions of CF and HF EHS stub columns with Class 4 cross-section ($D_e/t\varepsilon^2 > 90$)

Labeling	*2a* (mm)	*t* (mm)	*a/b*	*A* (mm^2)	R_{max}/t	$D_e/t\varepsilon^2$		A_{eff} (mm^2)	
						CF	HF	CF	HF
120×120×2	120.0	2.0	1.0	741	30.0	110.5	98.6	669.3	707.5
120×80×3	120.0	3.0	1.5	924	30.0	110.5	98.6	834.0	881.7
120×60×4	120.0	4.0	2.0	1114	30.0	110.5	98.6	1005.4	1062.9
120×48×5	120.0	5.0	2.5	1306	30.0	110.5	98.6	1179.1	1246.5
120×40×6	120.0	6.0	3.0	1499	30.0	110.5	98.6	1352.9	1430.2
270×270×5	270.0	5.0	1.0	4163	27.0	99.4	88.7	3960.8	4187.1
270×180×7	270.0	7.0	1.5	4845	28.9	106.5	95.1	4454.0	4708.5
270×135×9	270.0	9.0	2.0	5639	30.0	110.5	98.6	5090.1	5380.9
270×108×11	270.0	11.0	2.5	6474	30.7	113.0	100.8	5778.7	6108.9
270×90×13	270.0	13.0	3.0	7325	31.2	114.7	102.4	6488.9	6859.6
420×420×7	420.0	7.0	1.0	9082	30.0	110.5	98.6	8198.5	8666.9
420×280×11	420.0	11.0	1.5	11840	28.6	105.4	94.1	10939.5	11564.6
420×210×14	420.0	14.0	2.0	13645	30.0	110.5	98.6	12316.8	13020.5
420×168×18	420.0	18.0	2.5	16432	29.2	107.4	95.9	15043.2	15902.7
420×140×21	420.0	21.0	3.0	18360	30.0	110.5	98.6	16573.3	17520.2
570×570×10	570.0	10.0	1.0	17593	28.5	104.9	93.7	16293.4	17224.4
570×380×14	570.0	14.0	1.5	20492	30.5	112.4	100.4	18334.6	19382.2
570×285×19	570.0	19.0	2.0	25131	30.0	110.5	98.6	22685.5	23981.7
570×228×24	570.0	24.0	2.5	29764	29.7	109.3	97.6	27008.9	28552.1
570×190×28	570.0	28.0	3.0	33263	30.5	112.4	100.4	29761.8	31462.3

Table 12: Dimensions of HF EHS stub columns
with Class 4 cross-section ($D_e/t\varepsilon^2 > 90$)

Labeling	*2a* (mm)	*t* (mm)	*a/b*	*A* (mm^2)	R_{max}/t	A_{eff} (mm^2)	$D_e/t\varepsilon^2$
120×120×1	120.0	1.0	1.0	374	60.0	252.6	197.2
120×60×2	120.0	2.0	2.0	569	60.0	384.5	197.2
120×40×3	120.0	3.0	3.0	776	60.0	523.9	197.2
270×180×4	270.0	4.0	1.5	2806	50.6	2063.7	166.4
270×135×5	270.0	5.0	2.0	3194	54.0	2274.1	177.5
270×108×6	270.0	6.0	2.5	3621	56.3	2526.1	184.9
420×420×4	420.0	4.0	1.0	5228	52.5	3775.4	172.6
420×210×7	420.0	7.0	2.0	6972	60.0	4709.6	197.2
420×168×9	420.0	9.0	2.5	8457	58.3	5794.2	191.7
570×570×5	570.0	5.0	1.0	8875	57.0	6151.3	187.3
570×380×7	570.0	7.0	1.5	10398	61.1	6962.6	200.7
570×285×10	570.0	10.0	2.0	13501	57.0	9357.6	187.3
570×228×12	570.0	12.0	2.5	15311	59.4	10397.5	195.2
570×190×14	570.0	14.0	3.0	17202	61.1	11518.2	200.7

Table 13: Comparison of parametric results with predicted strengths for CF and HF EHS with $D_e/t\varepsilon^2 \leq 50$

Labeling	CF				HF			
	P_{FEA} (kN)	$P_{FEA}/P_{C\&G}$	P_{FEA}/P_{DSM}	$P_{FEA}/P_{C\&Y}$	P_{FEA} (kN)	$P_{FEA}/P_{C\&G}$	P_{FEA}/P_{DSM}	$P_{FEA}/P_{C\&Y}$
120×120×5	1080	1.38	1.38	1.20	1007	1.44	1.44	1.24
120×60×10	1820	1.62	1.62	1.36	1711	1.70	1.71	1.42
270×270×12	5903	1.40	1.40	1.21	5523	1.47	1.47	1.25
270×180×17	7458	1.53	1.54	1.30	7014	1.62	1.62	1.35
420×420×18	12960	1.32	1.32	1.14	11934	1.36	1.36	1.16
570×570×24	23585	1.32	1.33	1.15	21746	1.37	1.37	1.17
Mean, P_m		1.43	1.43	1.23		1.49	1.50	1.27
COV, V_P		0.084	0.085	0.069		0.093	0.093	0.079

Table 14: Comparison of parametric results with predicted strengths for CF and HF EHS with $50 < D_e/t\varepsilon^2 \leq 70$

Labeling	CF				HF			
	P_{FEA} (kN)	$P_{FEA}/P_{C\&G}$	P_{FEA}/P_{DSM}	$P_{FEA}/P_{C\&Y}$	P_{FEA} (kN)	$P_{FEA}/P_{C\&G}$	P_{FEA}/P_{DSM}	$P_{FEA}/P_{C\&Y}$
120×120×3.5	701	1.26	1.27	1.14	630	1.27	1.27	1.12
120×60×7	1171	1.44	1.44	1.26	1085	1.49	1.49	1.29
270×270×8	3689	1.30	1.30	1.15	3403	1.34	1.34	1.17
270×135×16	6116	1.46	1.46	1.28	5664	1.51	1.52	1.31
420×420×12	8086	1.22	1.22	1.08	7272	1.22	1.23	1.08
420×280×19	11860	1.37	1.37	1.19	11006	1.43	1.43	1.22
570×570×17	15789	1.24	1.24	1.10	14319	1.26	1.26	1.10
570×380×26	22061	1.38	1.38	1.20	20463	1.43	1.43	1.23
Mean, P_m		1.33	1.33	1.18		1.37	1.37	1.19
COV, V_P		0.069	0.070	0.059		0.081	0.082	0.072

Table 15: Comparison of parametric results with predicted strengths for CF and HF EHS with $70 < D_e/t\varepsilon^2 \leq 90$

Labeling	CF				HF			
	P_{FEA} (kN)	$P_{FEA}/P_{C\&G}$	P_{FEA}/P_{DSM}	$P_{FEA}/P_{C\&Y}$	P_{FEA} (kN)	$P_{FEA}/P_{C\&G}$	P_{FEA}/P_{DSM}	$P_{FEA}/P_{C\&Y}$
120×80×4	682	1.29	1.29	1.16	606	1.29	1.29	1.14
120×60×5	772	1.30	1.30	1.17	677	1.27	1.28	1.13
270×270×6	2535	1.18	1.18	1.08	2202	1.15	1.15	1.04
270×135×12	4255	1.33	1.33	1.19	3799	1.33	1.33	1.17
420×420×9	5805	1.15	1.16	1.06	4963	1.11	1.11	1.01
420×280×14	8211	1.27	1.27	1.14	7206	1.25	1.25	1.11
420×210×19	10421	1.32	1.33	1.18	9286	1.32	1.32	1.16
570×570×13	11251	1.14	1.14	1.05	9621	1.10	1.10	0.99
570×380×19	15117	1.27	1.27	1.14	13279	1.25	1.25	1.11
570×285×25	18488	1.31	1.31	1.17	16313	1.30	1.30	1.15
Mean, P_m		1.26	1.26	1.13		1.23	1.24	1.10
COV, V_P		0.056	0.057	0.045		0.070	0.071	0.060

Table 16: Comparison of parametric results with predicted strengths for CF and HF EHS with $D_e/t\varepsilon^2 > 90$

Labeling	CF				HF			
	P_{FEA} (kN)	$P_{FEA}/P_{C\&G}$	P_{FEA}/P_{DSM}	$P_{FEA}/P_{C\&Y}$	P_{FEA} (kN)	$P_{FEA}/P_{C\&G}$	P_{FEA}/P_{DSM}	$P_{FEA}/P_{C\&Y}$
120×120×2	356	1.23	1.11	1.05	301	1.10	1.05	0.98
120×80×3	482	1.34	1.21	1.12	395	1.16	1.11	1.01
120×60×4	587	1.35	1.22	1.12	497	1.21	1.16	1.05
120×48×5	714	1.40	1.27	1.17	615	1.28	1.22	1.11
120×40×6	861	1.47	1.34	1.22	767	1.39	1.33	1.20
270×270×5	2049	1.20	1.14	1.06	1741	1.08	1.08	0.99
270×180×7	2573	1.34	1.23	1.13	2138	1.18	1.14	1.04
270×135×9	2989	1.36	1.23	1.13	2538	1.22	1.17	1.06
270×108×11	3522	1.41	1.26	1.16	3021	1.28	1.21	1.10
270×90×13	4230	1.51	1.34	1.23	3860	1.46	1.37	1.24
420×420×7	4234	1.19	1.08	1.02	3597	1.07	1.03	0.95
420×280×11	6132	1.30	1.20	1.10	5031	1.13	1.10	1.00
420×210×14	7236	1.36	1.23	1.13	5902	1.17	1.12	1.02
420×168×18	9044	1.39	1.28	1.17	7849	1.28	1.24	1.12
420×140×21	10521	1.47	1.33	1.22	9381	1.39	1.33	1.20
570×570×10	8287	1.18	1.09	1.02	6992	1.05	1.03	0.96
570×380×14	10441	1.32	1.18	1.09	8522	1.14	1.08	0.98
570×285×19	13308	1.36	1.23	1.13	10851	1.17	1.12	1.01
570×228×24	16287	1.39	1.27	1.16	14055	1.27	1.23	1.11
570×190×28	18940	1.47	1.33	1.21	16813	1.38	1.32	1.19
Mean, P_m		1.35	1.23	1.13		1.22	1.17	1.07
COV, V_P		0.071	0.065	0.057		0.096	0.090	0.083

Table 17: Comparison of parametric results with predicted strengths for HF EHS with $D_e/t\varepsilon^2 > 90$

Labeling	P_{FEA} (kN)	$P_{FEA}/P_{C\&G}$	P_{FEA}/P_{DSM}	$P_{FEA}/P_{C\&Y}$
120×120×1	146	1.50	1.01	1.01
120×60×2	226	1.52	1.03	1.00
120×40×3	314	1.55	1.05	1.02
270×180×4	1116	1.40	1.03	0.99
270×135×5	1277	1.45	1.04	1.00
270×108×6	1460	1.50	1.05	1.01
420×420×4	2043	1.40	1.01	1.00
420×210×7	2772	1.52	1.03	1.01
420×168×9	3406	1.52	1.05	1.01
570×570×5	3464	1.46	1.01	1.01
570×380×7	4111	1.53	1.03	1.00
570×285×10	5391	1.49	1.04	1.00
570×228×12	6159	1.53	1.05	1.01
570×190×14	6948	1.56	1.05	1.02
Mean, P_m		1.50	1.03	1.01
COV, V_P		0.034	0.014	0.008

Table 18: Summary of comparison of test and numerical results with predicted strengths

	CF				HF			
	Test + FEA	$P_u/P_{C\&G}$	P_u/P_{DSM}	$P_u/P_{C\&Y}$	Test + FEA	$P_u/P_{C\&G}$	P_u/P_{DSM}	$P_u/P_{C\&Y}$
Mean, P_m	13 + 44	1.32	1.24	1.12	26 + 58	1.30	1.17	1.06
COV, V_P		0.105	0.111	0.092		0.128	0.138	0.105
ϕ_1		1.00	0.85	0.85		1.00	0.85	0.85
β_1		2.89	3.36	3.07		2.72	3.01	2.82
ϕ_2		0.85	0.85	0.85		0.85	0.85	0.85
β_2		3.66	3.36	3.07		3.46	3.01	2.82